

Is there anything left? Measuring semantic residuals of objects removed from 3D Gaussian Splatting

Simona Kocour^{1,2}

Assia Benbihi²

Aikaterini Adam³

Torsten Sattler²

¹Faculty of Electrical Engineering, Czech Technical University in Prague

²Czech Institute of Informatics, Robotics and Cybernetics, Czech Technical University in Prague

³Archimedes/Athena RC

simona.kocour@cvut.cz

Abstract

Searching in and editing 3D scenes has become extremely intuitive with trainable scene representations that allow linking human concepts to elements in the scene. These operations are often evaluated on the basis of how accurately the searched element is segmented or extracted from the scene. In this paper, we address the inverse problem, that is, how much of the searched element remains in the scene after it is removed. This question is particularly important in the context of privacy-preserving mapping when a user reconstructs a 3D scene and wants to remove private elements before sharing the map. To the best of our knowledge, this is the first work to address this question. To answer this, we propose a quantitative evaluation that measures whether a removal operation leaves object residuals that can be reasoned over. The scene is not private when such residuals are present. Experiments on state-of-the-art scene representations show that the proposed metrics are meaningful and consistent with the user study that we also present. We also propose a method to refine the removal based on spatial and semantic consistency. The evaluation framework and data are available at https://github.com/simonakocour/anything_left

1. Introduction

Trainable scene representations, such as neural radiance fields (NeRFs) [14, 22, 42, 57, 58, 63, 76] or 3D Gaussians [25, 37, 43, 50, 93, 101, 104], enable photorealistic 3D reconstructions from images. They are gaining tremendous popularity thanks to the high quality of the reconstructed geometry and the realism of the renderings.

These learnable scene representations can be easily extended to include features that carry semantic meaning [33,

36, 38, 84, 95, 97, 106]. This, in turn, creates a link between parts of the scene and human understandable concepts in general and human language in particular. This link can then be used for intuitive search in 3D scene representation by prompting [34, 41, 48, 67, 87], e.g., asking 'find the remote control'. Similarly, it enables intuitive editing operations [24, 26, 32, 97, 106], e.g., by asking to 'remove the red armchair in the living room'.

The growing availability of learning-based 3D reconstruction software accessible to nonexpert users [2–4, 6, 75, 88, 98, 100], coupled with intuitive edit operations based on natural language [9, 70, 83], opens up exciting possibilities: using data casually captured by a smart phone [2, 3, 5, 6], a user can easily create and edit photorealistic 3D models. In particular, they can remove parts of the scene that they consider private, e.g., photos, documents, types of decoration, etc., before sharing these maps, e.g., before uploading them to online services for refurbishing¹. The privacy implications of sharing 3D maps naturally lead to questions on how well existing approaches for intuitive edit operations perform.

This paper is dedicated to this privacy aspect of (language-based) editing of trainable scene representations. We focus on removing objects from scenes and investigating whether state-of-the-art removal methods leave residuals that enable us to reason about what content was removed. Contrary to previous works [19, 27, 60] that focus on foreground / background segmentation, we are interested in whether the residuals of the objects remain in the scene after removal and whether the residuals can be reasoned over. To the best of our knowledge, this is the first

¹As an example, IKEA provides an app that allows users to scan rooms. The captured data is uploaded to IKEA's servers. Hence, IKEA recommends to physically remove private parts before scanning. In contrast, the systems envisioned in this paper allow to perform the removal virtually after the scan, which is more practical and less physically demanding.



Figure 1. **Is there any table left after it is removed from the scene?** When there remain residuals of the object, and they can be reasoned over (left column, mid-row), the object removal is imperfect. This is what the proposed evaluation measures based on whether off-the-shelf semantic models can still segment the object after the removal. We also measure the presence of residuals in 3D with depth (right column, mid-row). We derive an optimization to refine the removal based on spatial and semantic consistency (highlighted in pink the bottom-left image). Top-Bottom: Rendering from the original 3DGS [37] scene, rendering after removing the table from the scene, rendering after removal and refinement. Left-Right: RGB renderings, SAM [39] masks overlay with pseudo-ground-truth object outline, GroundedSAM [39, 54, 77] overlay, depth renderings.

work that considers this aspect of trainable scene representations. Hence, this paper focuses on introducing an evaluation framework to quantitatively and qualitatively measure how well the current state-of-the-art methods remove objects from the scene. We propose metrics that measure how well an object is recognized after removal using off-the-shelf semantic segmentation at various granularity levels (object semantics, instances, and object parts) and 3D perception with depth. Experiments on indoor and outdoor scenes show that the proposed metrics are consistent in their ranking of the evaluated methods. Also, their complementarity makes the proposed evaluation robust to errors in the semantic segmentations. We complete the quantitative results with qualitative insights drawn from a user study with human volunteers that evaluate the removal methods. The human conclusions are mostly consistent with the quantitative metrics we define. We also derive a graph-based optimization to refine the removal that leverages the tight coupling between the geometry and the semantics of the scene. Results show that the refinement either preserves or improves the quality of the object removal. In summary, our contributions are: i) we propose an evaluation that measures how well scene removal operations remove objects in the context of privacy. To the best of our knowledge, this

is the first work that considers this aspect of trainable scene representations; ii) we define quantitative metrics to enable this evaluation and demonstrate their soundness on state-of-the-art trainable scene representations; iii) we complete our quantitative evaluation with a user study that draws insights consistent with the metrics; iv) we define a graph-based optimization that refines the object removal by enforcing spatial and semantic consistency in the removal. The code and the data used in the evaluation are available at https://github.com/simonakocour/anything_left

2. Related Work

3D reconstruction from images builds 3D models that capture the scene’s geometry and appearance. Popular scene representations are point clouds [34, 51, 67, 81, 99, 102], meshes [28, 44, 45, 82], and, more recently, Neural Radiance Fields (NeRFs) [14, 22, 42, 57, 58, 63, 76] and 3D Gaussian Splatting (3DGS) [25, 37, 43, 50, 93, 101, 104].

NeRFs represent the scene implicitly with a colored volumetric field: for each 3D point in the space, an MLP outputs a volumetric density and a view-dependent color value. NeRFs are optimized for novel-view synthesis, *i.e.*, so that a rendering of the field from a given view is similar to the original image from that view. In 3DGS [37], the scene is

represented explicitly with a set of 3D Gaussians with learnable parameters (positions, orientation, scale, opacity, view-dependent color). Again, the parameters are optimized so that splatting, *i.e.* rendering, the Gaussians generates a rendering that is similar to the original view.

Linking 3D reconstructions and semantics. NeRFs and 3DGS can easily be extended to embed semantic features that can be prompted via natural language [38, 89], pixel locations [38, 89] or semantic labels [97]. The prompt allows humans to search for elements in the 3D reconstruction then edit that location. The type of prompt and the edition operation depend on the 3D representation and the embedded semantic features.

In NeRFs, the MLP is extended to output semantic features that are rendered in a differential manner (as for the color) and supervised with off-the-shelf 2D semantic features. Examples are NeRFs extended with text features [59, 92] like CLIP [70], text and semantic features [38, 40], and unsupervised features [89] like DINO [18, 66]. Prompting for an element in the reconstruction amounts to finding the features in the NeRF field that are the most similar to the prompt’s features. The feature field can also be trained to render segmentation masks consistent with 2D masks [20, 55, 91, 105] derived with semantic models [23, 29, 46], panoptic models [15, 85], foundation models [39, 47, 52, 74, 107], or user annotations [60]. The prompt search then looks for the features associated with a given semantic label.

Although these methods perform well in locating prompted elements in the reconstruction, the implicit nature of NeRFs makes it complex to associate a location in the reconstruction with a set of abstract MLP parameters to edit. Hence, editing the reconstruction is not as straightforward as in 3DGS [37] representations that are explicit: removing a prompted location amounts to deleting the 3D Gaussians at that location. 3DGS can also be embedded with semantic features as easily as NeRFs with semantic models [19, 27, 32, 36, 96, 106], text features [49, 69, 84], and unsupervised features [108]. This motivates this paper to focus on 3D reconstructions represented with 3DGS [37].

Evaluating 3D reconstruction approaches. 3D reconstructions are evaluated based on the accuracy of the 3D geometry and whether the color renderings and the semantic (features) renderings are similar to those in the training views.

Often, scene operations, such as editing and removal, are reported only as illustrative examples with qualitative results [27, 32, 36, 96, 97, 106]. Some works [19, 27, 60] report a quantitative evaluation of ‘background’ removal by comparing the renderings of the searched element against its appearance in the original view. This paper addresses a different problem, *i.e.*, are there residuals of the removed object in the scene and if so, can they still be recognized or

reasoned over? We propose an evaluation framework to answer this question in a quantitative and automatic manner. To the best of our knowledge, there is no previous work that addresses such a question.

Privacy challenges. The use of extensive public data in the recent scientific breakthroughs [9, 17, 78, 80] has drawn attention to the protection of user data in the research community [21, 61, 65, 68, 73, 86], in companies [31, 79], and governments [35, 90].

This challenge will grow as the deployment in households of new types of sensors, *e.g.*, Augmented Reality / Virtual Reality (AR / VR) glasses [1, 7, 8], and autonomous systems will become the norm. An efficient way to make systems privacy-preserving is to consume data that has already been made privacy-preserving by the user. One relevant line of work proposes to anonymize the images [56, 94] with inpainting before the scene reconstruction rather than editing the reconstruction later.

However, this method is more computationally complex: it involves editing many images as opposed to a single reconstruction and can introduce artifacts in the image that reduce the quality of the reconstruction. Hence, operating on the 3D model offers privacy at a reasonable computational cost and better reconstruction quality.

3. Metrics Definition

We evaluate whether removal operations in 3DGS [37] leave information about the removed content. The proposed evaluation is conducted in the context of privacy considerations raised when sharing the scene representations. Within this context, an element is considered private if it can not be identified [35, 73, 90].

This section defines the metrics that evaluate whether elements can be identified after removal.

3.1. Semantic Object Recognition

Semantic segmentation identifies objects in the scene by classifying each pixel into semantic categories [23, 29, 46]. Here, it is used to assess whether an object can be identified by rendering the scene from multiple views and measuring the performance of the segmentation model on those renderings. Comparing the segmentation performance before and after removal provides information on the removal quality. A drop in performance indicates that the object is removed.

We thus define the semantic recognition metric as the segmentation’s performance gap on the renderings before and after removal.

The semantic segmentation is evaluated with the standard Intersection over Union (IoU) [12, 23] that measures how well the estimated semantic mask overlaps with the ground-truth mask.

We compute IoU_{pre} and IoU_{post} on the masks estimated on the renderings before and after removal, respectively.

The IoU drop IoU_{drop} is defined as:

$$\text{IoU}_{\text{drop}}^{\uparrow} = \text{IoU}_{\text{pre}} - \text{IoU}_{\text{post}} \quad (1)$$

IoU_{drop} ranges between 1 and -1 and the higher, the better the object is removed, as indicated by the \uparrow .

Low absolute value of the IoU_{drop} implies that $\text{IoU}_{\text{post}} = \text{IoU}_{\text{pre}}$, which can be interpreted in two ways. (1) Both $\text{IoU}_{\text{post,pre}}$ are high, *i.e.*, the segmentation model identifies the object both before and after removal, so the removal failed. (2) When both IoUs are low, no conclusion can be drawn since the segmentation model could not segment the object even in the original image. Thus, there is no performance drop to measure.

To address the ambiguity between these two interpretations, we complete this metric with another semantic metric defined in the next section.

Still, IoU_{drop} is relevant on its own to signal an issue with the removal or the evaluation, which can be useful in systems with a man in the loop, *e.g.*, active labeling.

In the experiments, we also report a more intuitive metric, the performance of the segmentation after removal, and analyse its correlation IoU_{drop} . We define the accuracy acc_{seg} as the ratio of test images in which the semantic element is not recognized anymore.

The element is not recognized if IoU_{post} is smaller than a given threshold ξ_{IoU} , and we report this metric over multiple thresholds. $\text{acc}_{\text{seg}}^{\uparrow}$ ranges between 0 and 1 and the higher acc_{seg} , the better the object removal, as indicated by the \uparrow .

$$\text{acc}_{\text{seg}, \xi_{\text{IoU}}}^{\uparrow} = \frac{\|\# \text{ images with } \text{IoU}_{\text{post}} < \xi_{\text{IoU}}\|}{\|\# \text{ images}\|} \quad (2)$$

3.2. Anything Recognition

The previous sections defined the IoU_{drop} that can be interpreted in two ways when it is low. To address such ambiguity, we complement the IoU_{drop} with a second semantic metric based on finer segmentations, *i.e.*, object parts or instances instead of semantic categories. These segmentations are derived with the foundational SegmentAnything (SAM) [39, 74],

a prompt-based segmentation model that can be prompted with image locations, bounding boxes, or texts.

The model can also operate without prompts, which results in a set of masks that cover all the semantic elements in the image (See Fig. 2).

In this evaluation, we assess whether an element has been removed by comparing the SAM [39, 74] masks of the scene renderings before and after removal. When the object is removed or partially removed, SAM segments what is behind the object so the masks should change (See rows 1 and 4 in Fig. 2).



Figure 2. SAM [39, 74] masks before and after object removal. Left-right: before and after removal. Rows: The evaluated methods. When the object (green outline) is removed (row 1 and 4), the SAM masks change, which is the signal we exploit to evaluate the removal: larger changes indicate better removal.

We next define sim_{SAM} that measures the similarity between two sets of SAM [39, 74] masks based on how well they spatially overlap.

We first match the masks that overlap the most between the two sets. Then sim_{SAM} is the average overlap between the mask matches. We enforce a 1-to-1 matching, *i.e.*, a mask in one set is matched to at most one mask in the other. We do so by defining that two masks match if they overlap, and if one mask gets matched to more than one, we keep the match that leads to the maximum overlay over all matches. This is derived by solving an assignment problem that maximizes the overlay over all matches with the Hungarian algorithm [64].

More formally, let $A = (a_i)_{i \in [1, N]}$ and $B = (b_j)_{j \in [1, M]}$ be the sets of SAM masks before and after object removal,

and $(a_k, b_k)_{k=1, K}$ be the K matching masks. The simi-



Figure 3. **Depth Changes before and after removal.** Left to right: original rendered depth, rendered depth after removal, thresholded depth difference and pseudo-ground-truth outline of the object to be removed in green. Top: GaussianCut [36] shows precise and localized changes in the depth maps, indicating accurate object removal. Down: Feature3DGS [106] fails to remove the object and the difference at the object location remains unchanged.

ilarity between the two sets of SAM masks A and B is:

$$\text{sim}_{\text{SAM}}^{\downarrow} = \frac{\sum_{k=1}^K \text{IoU}(a_k, b_k)}{\max(N, M)} \quad (3)$$

$\text{sim}_{\text{SAM}}^{\downarrow}$ lies in $[0, 1]$ and the lower the score, the less similar the masks, hence the better the removal, as indicated by the \downarrow .

Note that we normalize the score with the highest number of masks $\max(N, M)$ instead of the number of mask matches K . We do so to account not only for the difference in overlay (in the numerator) but also for the difference in the number of masks. To reflect the changes related to the removed object, the metric is derived only over the masks that overlay with the object with an IoU of at least 0.1.

3.3. Spatial Recognition

We complete the previous metrics with one that depends only on the 3D scene before and after removal, hence increasing the robustness of the evaluation against possible errors in the segmentations.

Inspired by recent works in scene change detection [10], we measure how well an object is removed based on the changes in the rendered depths before and after removal: a strong change in the depth maps indicates a change in the scene.

Hence, if the depth of the object changes enough, then the object is well removed.

More formally, we report the ratio of the object’s pixels which depth changes by more than a threshold ξ_{depth} . The

threshold ξ_{depth} is derived automatically with Generalized Histogram Thresholding [13] on the histogram of depth differences over the whole image (See Fig. 3).

The depth maps are derived from the scene’s rendering before and after removal so they have consistent scales. The defined ratio can be interpreted as the accuracy in depth change and is noted $\text{acc}_{\Delta\text{depth}}$:

$$\text{acc}_{\Delta\text{depth}}^{\uparrow} = \frac{\#\text{object pixel with depth change} > \xi_{\text{depth}}}{\#\text{object pixels}} \quad (4)$$

The object’s pixel locations are specified by the object’s mask in the image that we assume is available.

3.4. Removal Refinement

Parts or residuals of an object can remain in the scene, even after removal. To address this issue, we propose a graph-based refinement that leverages the tight coupling between the geometry and the semantics of the scene [11, 53, 62].

After a method outputs a set of Gaussians to be removed, the refinement looks for other Gaussian candidates for removal within the spatial and semantic neighborhood of that set. The refinement defines a graph over all 3D Gaussians and partitions them into one set to be removed and one to remain. The sets are initialized with the output of the removal method and refined to optimize the semantic and spatial consistency of the partitions. This is done by finding a graph cut with maximum spatial and semantic consistency [16, 30, 103]. Such a graph-based optimization is also used in GaussianCut [36] to segment the foreground

and background elements in the scene. The proposed refinement differs in the graph definition and the energy cost. In [36] the correlation between two Gaussians depends on their spatial proximity and their color similarity. Here, the correlation between two Gaussians depends not only on their spatial proximity, as in [36], but also their semantic similarity. Next, we formalize the graph definition and the energy cost minimized in the graph-cut algorithm.

The graph’s nodes are the 3D Gaussians and edges are drawn between spatially close Gaussians. To reduce the size of the graph optimization, we filter out the Gaussians that do not ‘intersect’ with the initial set of Gaussians to be removed. Two Gaussians are said to ‘intersect’ if the Euclidean distance between their centers is smaller than the sum of their largest scale. This is equivalent to approximating the Gaussians as spheres and testing for the spheres’ intersections. Next, the edges are based on the spatial distance and feature similarity between the nodes. The spatial distance between two Gaussians is defined as the Euclidean distance between their centers. A node has edges with the nodes among its K nearest neighbors that also have a feature similarity higher than a threshold δ . The partition that optimizes the spatial and semantic consistency between nodes is the partition that minimizes the energy cost defined with two terms: the unary terms represent the likelihood of a Gaussian to be removed, and the binary term represents the semantic consistency between neighboring Gaussians. The unary term is initialized with respectively 1 or 0 based on whether the Gaussian is removed or not by the method being refined. The binary term between two Gaussian is their semantic similarity measured with the L2 distance between their semantic features.

4. Experiments

We compare various Gaussian-based scene representations under the proposed metrics on indoor and outdoor scenes.

Approaches. We evaluate the **Feature3DGS (FGS)** [106] variant that distills the LSEG [46] semantic features aligned with CLIP’s text features [70]. FGS is prompted with a tuple of text entries: one positive query is associated with the object of interest and the others are negative queries. The search compares the Gaussians’ feature with the features of each text entry, and their similarity is normalized. The Gaussian is removed if the similarity with the query text prompt is higher than 0.4.

GaussianGrouping (GG) [97] distills SAM [39] semantic features that operate at a finer granularity than LSEG [47]. Also, GG enforces spatial consistency between semantically similar Gaussians so that close-by Gaussians have similar features. Prompting is less intuitive than in FGS [106], as one can only query one of the SAM instance labels present in the training views. A Gaussian is removed if its feature is associated with the prompted instance label.

Post-processing then removes all Gaussians within the convex hull of the removed Gaussians.

SAGS [33] is a training-free and feature-free method that takes object masks as prompts.

It estimates a removal probability for each Gaussian based on projective geometry.

The 3D center of the Gaussian is projected on the images and the removal probability is the ratio of images in which the projections land on the object’s location.

If the probability is higher than 0.7, the Gaussian is removed. SAGS regularizes the removal to better fit the actual object’s boundaries by splitting the Gaussians around the boundary and only removing the splits within the boundary. Although efficient, using projective geometry instead of splatting [37] when assigning Gaussians to the object does not account for the Gaussian’s opacity, which may lead to over-removal.

GaussianCut (GC) [36] is also a feature-free and training-free method that leverages the spatial and color correlations between Gaussians.

Given a trained 3DGS [37] scene, it models the scene as a graph and determines which Gaussians should be removed via graph optimization.

As for SAGS, the prompt is a set of object masks.

The Gaussians define the nodes of the graph and are extended with a single parameter representing the probability of the Gaussian to be removed. The parameter is initialized by lifting the 2D prompt mask to 3D and refined via graph-cut optimization where the unary term represents the likelihood of the Gaussian to be removed and the binary term measures the color similarity and spatial distance between two Gaussians.

Dataset. The methods are compared on indoor and outdoor scenes of the mipNeRF360 dataset [14]. The dataset provides images with their camera poses and calibration but no ground-truth semantic masks necessary to derive the proposed metrics. Hence, we derive pseudo-ground-truth semantic masks for a set of objects using SAM [39] and human annotations (see Supp.).

Implementation Details. Some methods [97, 106] have large memory requirements that go beyond our computational resources. Thus, we select between 100 and 150 images from each scene. This does not affect the trained representations that can be trained from as little as 60 images [36] or 80 images [106]. All methods are trained on the same set of images and the same input 3D point cloud derived with Structure-from-Motion (SfM) using COLMAP [81]. The graph optimization uses the pcp library [71, 72]. The parameters of the graph refinement and of the evaluated methods are reported in the Supp. We use Grounded-SAM [39, 54, 77] to derive the metrics based on semantic segmentation.

Scene-Object	IoU _{drop} ↑				acc _{Δdepth} ↑				sim _{SAM} ↓			
	FGS	GG	SAGS	GC	FGS	GG	SAGS	GC	FGS	GG	SAGS	GC
Counter-Baking Tray	0.34	<u>0.53</u>	0.10	0.62	0.99	0.96	0.21	0.98	0.21	<u>0.35</u>	0.71	<u>0.35</u>
Counter-Plant	0.75	<u>0.84</u>	0.03	0.86	1.00	1.00	0.01	0.99	0.13	0.12	0.85	<u>0.13</u>
Counter-Gloves	0.01	0.60	0.10	0.60	0.01	1.00	0.55	1.00	0.99	0.12	0.56	<u>0.16</u>
Counter-Egg Box	0.08	0.63	0.56	<u>0.62</u>	0.06	1.00	0.86	1.00	0.84	0.15	0.47	<u>0.19</u>
Room-Plant	0.53	0.26	0.17	0.53	0.97	0.70	0.33	0.99	<u>0.22</u>	0.33	0.57	0.14
Room-Slippers	0.00	0.82	0.25	<u>0.48</u>	0.00	1.00	0.91	0.98	1.00	0.05	0.45	<u>0.35</u>
Room-Coffee table	0.57	0.86	0.00	0.86	0.67	0.89	0.06	0.99	0.26	<u>0.08</u>	0.86	0.07
Kitchen-Truck	0.62	0.61	0.67	<u>0.66</u>	0.96	1.00	1.00	0.92	0.35	<u>0.17</u>	0.22	0.08
Garden-Table	0.67	0.48	<u>0.81</u>	0.86	0.99	1.00	0.98	1.00	0.11	0.14	0.04	<u>0.06</u>
Garden-Ball	0.00	0.16	<u>0.41</u>	0.42	0.00	0.60	0.60	0.53	0.59	0.01	<u>0.21</u>	0.37
Garden-Vase	0.79	0.64	<u>0.96</u>	0.97	0.99	1.00	0.96	1.00	0.12	0.10	<u>0.11</u>	<u>0.11</u>

Table 1. **Object removal evaluation with the proposed metrics.** The three metrics measure changes in semantics and depth before and after removal: the $\text{IoU}_{\text{drop}}^{\uparrow}$ measures the drop in semantic segmentation, $\text{acc}_{\Delta\text{depth}}^{\uparrow}$ the changes in the depth maps, and $\text{sim}_{\text{SAM}}^{\downarrow}$ a change in the SAM [39] masks. The **best** and **second-best** are highlighted for $\text{IoU}_{\text{drop}}^{\uparrow}$ and $\text{sim}_{\text{SAM}}^{\downarrow}$. GaussianCut (GC) [36] and GaussianGrouping (GG) [97] mostly outperform Feature3DGS (FGS) [106] and SAGS [33].



Figure 4. **Segmentation changes before and after removal.** Left-right: GroundedSAM [39, 54, 77] overlay on the rendering before removal, rendering after removal, overlay after removal. The object is removed successfully but the segmentation model still finds it. One explanation can be that the pixel distribution on the edited area still exhibits patterns characteristic of the object, similar to what occurs in adversarial attacks. Even though the object can not be recognized by a human, GroundedSAM [39, 54, 77] still manages to segment the object.

4.1. Results

Methods comparison. Tab. 1 evaluates the considered approaches under our proposed metrics. The methods’ ranks remain stable across the three metrics: GaussianCut (GC) [36] and GaussianGrouping (GG) [97] achieve the best performances followed by SAGS [33] and Feature3DGS (FGS) [106]. GG and GC are mostly on par with GC reaching slightly higher $\text{IoU}_{\text{drop}}^{\uparrow}$ whereas GG has better $\text{sim}_{\text{SAM}}^{\downarrow}$. SAGS exhibit variance in the results: it gets on par with GC and even outperforms GG on the outdoor Garden scene but is often subpar on the rest of the scenes and objects. The performance of FGS also varies, although it does not appear correlated to the type of scene.

One property that GG [97] and GC [36] share is leveraging the spatial correlation of Gaussians to assess whether they belong to the same object. Their strong performance suggests that spatial consistency is an important property

for scenes to be suitable for search and edit operations. One advantage of GaussianCut [36] over GG [97] is its simplicity, and its memory and computational efficiency: it relies on a simple graph-cut optimization that can run on CPU and does not require distilling and storing semantic features into the 3DGS.

One explanation for the underperformance of FGS [106] may be that it is sensitive to the prompt. For example, if the tuple of text prompts is not contrastive enough or if the prompts are out of distribution, the similarity between the Gaussian’s feature and the prompt could be meaningless.

Another noticeable result is the gap between the indoor and outdoor performances of SAGS [33]. One explanation may be that the objects outdoors are well-separated spatially so the projective-geometry-based association between objects and Gaussians is accurate enough.

Complementarity analysis of the metrics. The ranking of the methods between the different metrics is mostly consis-

	$\text{acc}_{\text{IoU-post}>0.5}^{\downarrow}$			
	FGS	GG	SAGS	GC
Baking Tray	21.7	<u>8.5</u>	51.9	0.09
Plant	0	0.0	83.3	0
Blue Gloves	72.1	16.3	66.3	<u>17.3</u>
EggBox	80.4	0.0	4.1	<u>1</u>
Plant (room)	0	20	28	0
Slippers	98.5	14.7	72.1	<u>55.9</u>
Table	38.4	1	90.9	1
Truck	4.9	7.8	0	<u>0.05</u>
Table	29.7	45.9	<u>12.2</u>	4.7
Ball	6.1	0	0	0
Vase	10.8	21.6	0	0

Table 2. **Object removal evaluation** based on the segmentation after removal only. We report the ratio $\text{acc}_{\text{IoU-post}>0.5}^{\downarrow}$ of images in which the segmentation still segments the object with $\text{IoU} > 0.5$. A low value signals that the object is not found but says nothing about the reliability of the segmentation contrary to the proposed $\text{IoU}_{\text{drop}}^{\uparrow}$.

tent, which is expected since they are all designed to measure the removal quality (Tab. 1). The presence of redundancy in the metrics makes the proposed evaluation robust to potential errors in the semantic models used in the derivation. When a method achieves good results on all three metrics, then it is very likely that the removal succeeded and that the metrics are reliable. However, a mix of good and bad metric scores indicates that either the removal quality is low or that the segmentation used to derive $\text{IoU}_{\text{drop}}^{\uparrow}$ and $\text{sim}_{\text{SAM}}^{\downarrow}$ are incorrect, thus, the metric is not reliable.

For example, a low $\text{IoU}_{\text{drop}}^{\uparrow}$ alone can be interpreted in two ways: the removal failed or the segmentation model is not reliable. The latter happens when the object was not segmented even before the removal, *i.e.*, IoU_{pre} is low, and $\text{IoU}_{\text{drop}}^{\uparrow}$ is bound by this value, as discussed in Sec. 3.1. The other metrics help disambiguate between the two interpretations. In particular, the $\text{acc}_{\Delta\text{depth}}^{\uparrow}$ is a trustworthy indicator for failure cases because it tends to overestimate the quality of the removal. Then, when this metric is low, it is likely that the removal failed, *e.g.*, the performance of SAGS [33] on the ‘Baking Tray’, ‘Plant’ or ‘Coffee Table’.

Inversely, a high $\text{acc}_{\Delta\text{depth}}^{\uparrow}$ does not imply that the object is well removed since it overestimates the removal quality.

This is the case for GaussianGrouping [97] on the ‘Garden-ball’: the $\text{IoU}_{\text{drop}}^{\uparrow}$ at 0.16 is low, whereas the $\text{acc}_{\Delta\text{depth}}^{\uparrow}$ is at 0.60. The third metric can disambiguate such a case: in this example, the $\text{sim}_{\text{SAM}}^{\downarrow}$ at 0.01 suggests that the removal performs well. Then the low $\text{IoU}_{\text{drop}}^{\uparrow}$ does not indicate a low-quality removal but instead that the semantic segmentation is not reliable on this instance, which we visually confirmed.

	$\text{IoU}_{\text{drop}}^{\uparrow}$		$\text{acc}_{\Delta\text{depth}}^{\uparrow}$		$\text{sim}_{\text{SAM}}^{\downarrow}$	
	FGS	SAGS	FGS	SAGS	FGS	SAGS
Counter-Plant	+0	*	+0	*	+0	*
Counter-Egg Box	*	+0.04	*	+0.12	*	+0
Room-Plant	+0.03	+0.09	+0.01	+0.04	-0.06	+0
Room-Slippers	*	+0.17	*	+0	*	+0
Room-Coffee Table	+0	*	+0.11	*	-0.14	*
Kitchen-Truck	+0.04	*	+0	*	-0.21	*
Garden-Table	*	+0.09	*	+0.01	*	+0
Garden-Vase	+0.11	+0.01	+0.01	+0.04	+0	+0

Table 3. **Graph-based Removal Refinement.** We report the change in performance on FGS [106] and SAGS [33]. ‘+’ indicates an improvement and ‘-’ a drop in performance. Fail cases are reported with * and occur when the refinement graph can not be built from the output of the removal method.

This example illustrates how complementary the metrics are: they make the evaluation robust by catching the other metrics’ failure cases.

We compare the proposed metrics to a more intuitive metric: the ratio of images in which the object is still segmented out after removal, and the lower the ratio, the better the removal. An object is said to be segmented if the IoU is higher than a threshold in $\{0.5, 0.7, 0.9\}$. We report the metric as $\text{acc}_{\text{IoU-post}>0.5}^{\downarrow}$ for 0.5 in Tab. 2 and for the other thresholds in the supplementary. The results show that the $\text{acc}_{\text{IoU-post}>0.5}^{\downarrow}$ is correlated to the $\text{IoU}_{\text{drop}}^{\uparrow}$, which supports that the latter is also a measure of the removal quality. However, the $\text{IoU}_{\text{drop}}^{\uparrow}$ is more informative since it not only reports whether an object is removed but also whether the metric itself is reliable.

For example, FGS [106] achieves an $\text{acc}_{\text{IoU-post}>0.5}^{\downarrow}$ of 6.1 on the ‘Garden-ball’, *i.e.*, the object is not segmented out after removal. This could mean that the object removal is successful. However, the IoU before removal is also low, *i.e.*, the segmentation model can not find the object even in the original scene. In that case, it is the segmentation that is not reliable, which is signaled with a low $\text{IoU}_{\text{drop}}^{\uparrow}$ of 0.0: it tells that no conclusion can be drawn and the other metrics must be further analyzed.

Graph-based removal refinement. We evaluate the removal before and after refinement on the two methods that do not leverage spatial regularization: FGS [106] and SAGS [33]. The results in Tab. 6 show that the refinement either improves or preserves the removal’s quality measured by the $\text{IoU}_{\text{drop}}^{\uparrow}$ and the $\text{acc}_{\Delta\text{depth}}^{\uparrow}$ but can hinder the $\text{sim}_{\text{SAM}}^{\downarrow}$.

Also, the refinement fails when the graph can not be initialized. This occurs when the removal method being refined does not output a meaningful set of Gaussians to start from, *e.g.*, FGS [106] does not remove the ‘Counter-eggbox’ or the ‘Room-slippers’ as indicated by their low $\text{IoU}_{\text{drop}}^{\uparrow}$ at 0.08 and 0.0. The same occurs for SAGS [33] on the ‘Counter-plant’ and the ‘Room-coffee table’. The refinement can also fail outside of this scenario, *e.g.*, FGS [106]

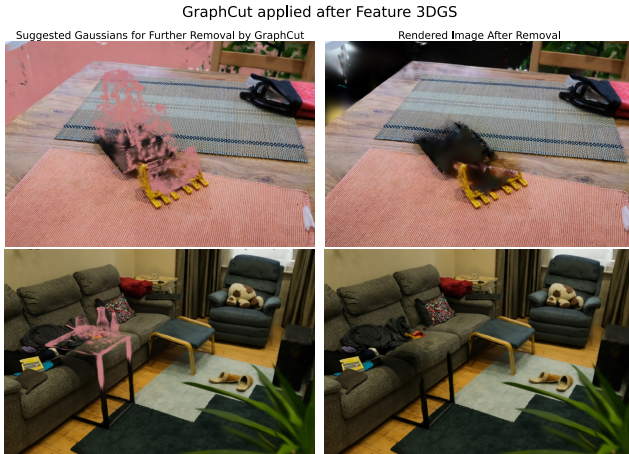


Figure 5. **Removal before and after refinement.** Left: removal before refinement. The area to be removed by the refinement is highlighted in pink. Right: removal after refinement. The refinement captures the object’s boundaries (top) and even relevant affordances, such as the elements on the tables to be removed.

on the ‘Garden-table’. Still, the refinement remains relevant as one can decide to include it or not based on whether it improves the metrics.

Qualitative Results. We show renderings of the evaluated methods before and after removal in Figs. 2 to 4. Fig. 4 illustrates an interesting use-case where the object is not visible to humans anymore, yet GroundedSAM [39, 54, 77] finds the object. This suggests that barely visible information about the object can remain in the scene, even when the removal is successful to the human eye, and that the proposed metrics can detect such scenarios. This opens interesting future directions on whether a network could be trained to invert the object removal from invisible pixel information and how to prevent it.

Fig. 5 shows the removal results of FGS [106] before (left) and after (right) the proposed graph-based refinement. The Gaussians removed by the refinement are colored pink on the left image and remain within the boundaries of the object. Fig. 2 shows the distribution of SAM [39] masks on the renderings of all methods before and after removal. It provides a visual intuition on how $\text{sim}_{\text{SAM}}^{\downarrow}$ behaves: GG [97] and GC [36] remove the ‘plant’ and the masks after removal and SAM [39] now segments the objects behind the plant. Conversely, the masks of FGS [106] and SAGS [33] before and after removal are similar because the removal failed. Fig. 3 provides a visual intuition for $\text{acc}_{\Delta\text{depth}}^{\uparrow}$ with a success (top) and failure case (bottom): when the object is well removed, there is a change in the rendered depth before and after removal at the location of the removed object (outlined in green). More visualizations are available in the supplementary.

User Study. We complete the previous analysis with a user

study with 8 volunteers. They evaluated the quality of the removal based on their ability to recognize the removed object, and their ability to detect whether an object has been removed. The users are presented with renders before and / or after removal and must answer the following questions: (1) Was an object removed from this image?; (2) Was an object removed from this specific area?; (3) Which method best removes the object?; (4) Does the graph-based refinement improve the removal? The questions are worded in a way to reduce potential bias, *e.g.*, in (1) and (2), the users are randomly shown images with no removal (see supplementary).

Overall, the conclusions of the study are consistent with the previous quantitative analysis: users find that Gaussian-Cut [36] performs best on 59% of the images, followed by GG [97] and SAGS [33] with 17%, then FGS [106] with 7%. This is in line with the quantitative results reported in Tab. 1. They also report that the graph-based refinement improves the removal. The participants can detect whether an object is removed in $\sim 88\%$ of the images, irrelevantly of the removal method and whether the removal area is highlighted or not. In the context of this paper, which focuses on the privacy aspect of the removal, a user being aware of the removal is not an issue as long as the removed content can not be identified. This is in line with existing privacy regulations, *e.g.*, the presence of blur in the images is fine as long as the faces and license plates are blurred [35, 90].

Limitations. The metrics rely on off-the-shelf semantic segmentation models that are prone to errors. Although introducing redundancy between the metrics alleviates this issue, it does not fully address it, which calls for further research on robust metrics for the evaluation of object removal.

5. Conclusion

We evaluate how well removal operations in 3DGS scenes perform in the context of privacy-preserving mapping by measuring whether there are residuals of the removed objects that can be reasoned over. To do so, we introduce an evaluation framework that measures whether the object can still be recognized after removal using off-the-shelf semantic models and 3D perception with depth. We test the proposed metrics on state-of-the-art scene representations, and results show that the proposed metrics are meaningful and consistent with a user study.

We also contribute a removal refinement based on spatial and semantic regularization. We hope this evaluation will contribute to fostering research towards better privacy-preserving representations.

Acknowledgements

This work was supported by the Czech Science Foundation (GACR) EXPRO (grant no. 23-07973X), the Ministry of Education, Youth and Sports of the Czech Republic through the e-INFRA CZ (ID:90254), the MIS 5154714 project of the National Recovery and Resilience Plan Greece 2.0 funded by the European Union under the NextGenerationEU Program.

Is there anything left? Measuring semantic residuals of objects removed from 3D Gaussian Splatting

Supplementary Material

The supplementary material provides additional implementation details, evaluation metrics, and extended experimental results supporting the main paper.

Section A describes the implementation details. Subsection A.1 presents the parameter settings for the compared methods: Feature3DGS [106], SAGS [33], GaussianGrouping [97], and GaussianCut [36]. Subsection A.2 details the evaluation metrics, including the generation of pseudo-ground-truth semantic masks. Subsection A.3 details the graph-cut refinement process, including its formulation and parameter settings.

Section B presents additional qualitative and quantitative results. Subsection B.1 reports the user study that evaluates the object removal quality and the impact of the graph-based refinement. Subsection B.2 reports the evaluation results of graph-based refinement. Subsection B.3 reports detailed results from the semantic IOU evaluation and the depth difference after object removal.

A. Implementation Details

A.1. Compared Methods

We use the official implementations provided by the respective authors and apply the following settings.

Feature3DGS (FGS) [106]. FGS is prompted with a tuple of text entries: one positive text prompt is associated with the object of interest and the others are negative text prompts. The search compares the Gaussians’ feature with the features of each text entry, and their similarity is normalized with softmax. We use the following negative prompts per scene: Garden: {grass, sidewalk, tree, house}, Room: {sofa, rug, television, floor}, Kitchen: {rug, table, chair}, Counter: {oranges, wooden rolling pin, coconut oil}. A Gaussian is removed if the similarity between the Gaussian’s feature and the prompt feature is higher than a threshold. We set this similarity threshold to 0.4 for all scenes and objects.

SAGS [33] is a training-free and feature-free method that takes object masks as prompts. It estimates a removal likelihood for each Gaussian based on projective geometry. The 3D center of the Gaussian is projected on the images and the removal probability is the ratio of images in which the projections land on the object’s location. A Gaussian is removed if its likelihood to be removed is higher than 0.7.

GaussianGrouping [97]. For the label training we set the SAM IoU prediction threshold to 0.8. For Gaussian training, we use default settings `densify_until_iter = 10000`,

`num_classes = 256`, `reg3d_interval = 5`, `reg3d_k = 5`, `reg3d_lambda_val = 2`, `reg3d_max_points = 200000`, `reg3d_sample_size = 1000`. For the object removal setting, we use the default number of classes of 256 and the removal threshold of 0.3.

GaussianCut [36] is also a feature-free and training-free method that leverages the spatial and color correlations between Gaussians. Given a trained 3DGS [37] scene, it models the scene as a graph and determines which Gaussians should be removed via graph optimization. As for SAGS, the prompt is a set of object masks. The Gaussians define the nodes of the graph and are extended with a single parameter representing the probability of the Gaussian to be removed. The parameter is initialized by lifting the 2D prompt mask to 3D and refined via graph-cut optimization where the unary term represents the likelihood of the Gaussian to be removed and the binary term measures the color similarity and spatial distance between two Gaussians. The graph is built with the following parameters: the number of edges is set to 10, the terminal cluster source is set to 5, the terminal cluster sink to 5, and the leaf size to 40. We use a foreground threshold of 0.9 and the prompt is a set of multi-view masks associated with the object to be removed.

A.2. Metrics

Pseudo-ground-truth semantic masks generation. Mip-NeRF360 [14] does not provide ground-truth semantic masks required for evaluation. Thus, we generate pseudo-ground-truth masks by running SAM [39] on images, segmenting all objects, and selecting the masks corresponding to the target objects. These masks are sufficiently accurate for evaluation. Since SAM [39] sometimes produces incomplete segmentation, we exclude the images with incomplete segmentation and use only fully segmented images.

Semantic Recognition. If Grounded-SAM [39, 54, 77] fails to detect an object for a given prompt, no semantic mask is produced, and the semantic IoU is 0.

A.3. Graph-Cut Refinement

We use FAISS [? ?] for nearest neighbor search in the graph refinement. The graph-cut algorithm [71, 72] minimizes a functional over a graph $G = (V, E)$ with total variation (d1) penalization, a separable loss term (we use smoothed Kullback-Leibler divergence loss), and simplex constraints

$$F(x) = f(x) + \|x\|_{d1} + \iota_{\text{simplex}}(x), \quad (5)$$

where:

	Nearest Neighbors K		Feature Similarity Threshold δ	
	FGS	SAGS	FGS	SAGS
Counter-Plant	10	*	0.8	*
Counter-Egg Box	*	10	*	0.8
Room-Plant	4	5	1.0	0.8
Room-Slippers	*	4	*	1.0
Room-Coffee Table	6	*	1.0	*
Kitchen-Truck	4	*	1.0	*
Garden-Table	*	10	*	0.8
Garden-Vase	4	10	1.0	0.8

Table 4. **Graph-based refinement parameters.** Graph parameters for different methods, scenes, and object removal. Failures, marked by “*”, occur when the constructed graph is empty, preventing further refinement.

- $x_v \in \mathbb{R}^D$ is the label for each vertex $v \in V$,
- $D = \{0, 1\}$ represents labels for removal (d=1) or retention (d=0),
- $f(x)$ is a separable data-fidelity loss,
- $\|x\|_{d1} = \sum_{(u,v) \in E} w_{d1_{uv}} \left(\sum_{d=0}^D w_{d1_d} |x_{ud} - x_{vd}| \right)$,
- $w_{d1_{uv}}$ is the weight of the edge between vertex u and v ,
- w_{d1_d} is the diagonal metric of the weights belonging to d -label.

The simplex constraint is defined as:

$$\iota_{\text{simplex}}(x) = \begin{cases} 0, & \text{if } x_{vd} \geq 0 \text{ and } \sum_d x_{vd} = 1, \forall v, d \\ \infty, & \text{otherwise} \end{cases} \quad (6)$$

Graph Construction and Parameters The graph nodes, edges, and cut parameters vary with respect to the scene, the removed object, and the removal method (Feature3DGS [106] or SAGS [33]). The parameters used for the graph construction are reported in Tab. 4.

The cut-threshold for determining Gaussian removal (1) or retention (0) is automatically set at the 95th percentile of the removal probability distribution. This means that the top 5% of Gaussian splats with the highest removal probabilities are removed, irrespective of their prior removal labels. Additional Gaussians for removal are identified by comparing the graph-cut removal labels with those from Feature3DGS [106] and SAGS [33], thereby refining the overall removal process.

B. Additional Results

B.1. User Study

Motivation. We complete the previous analysis with a user study with 8 volunteers. They evaluated the quality of the removal based on their ability to recognize the removed object, and their ability to detect whether an object has been removed. The users are presented with renders before and / or after removal and must answer the following questions. We describe the ‘Goal’ of the question, *i.e.*, what we evaluate, the ‘Display’, *i.e.*, what content is shown to the user,

and the ‘Question’ asked to the user.

Q1. Goal: Assess the removal success and assess whether potential removal artifacts are similar to “regular” artifacts in the renderings? To avoid biasing the study by showing only images with removed elements, hence biasing the user to answer only ‘yes’, images before removal are also shown with a random probability.

Display: an image of the render before or after object removal.

Question: Was an object removed from this image?

Q2. Goal: Asses the removal success in a region of the image.

Display: an image of the render after object removal and with a box drawn around the object area so that the user focuses on that particular area. Again, to avoid biasing the study by showing only images with removed elements, images before removal are also shown with a random probability.

Question: Was an object removed from this area?

Q3. Goal: Compare the removal from several methods and assess whether the associated metrics on that image are consistent with the human assessment.

Display: an image of the render after object removal with a box drawn around the object area. We display the results from several methods next to each other.

Question: In which image is the object best removed?

Q4. Goal: Assess whether the proposed graph-cut refinement improves the removal.

Display: an image of the render after object removal but before refinement, and after both the removal and the refinement.

Question: In which image is the object best removed?

Results: 97% of the users picked the image after graph-cut refinement, which supports that the refinement makes the removal visually better.

Results. We show examples of images shown in the user study in Fig. 6 for Q1, in Fig. 7 for Q2, in Fig. 8- Fig. 11 for Q3, and in Fig. 12, Fig. 13 for Q4. The caption describes the users’ conclusion for each instance. Overall, user responses align with the proposed metrics, which supports the soundness of the metrics. Tab. 5 presents object-wise results aggregated from Q4: which method best removes the object? For each object, we report the ratio of votes accumulated over multiple images and all users. ‘-’ indicates that no user has voted for a given method. The users often find that GaussianCut [36] is the best followed by Gaussian-Grouping [97] and SAGS [106].

B.2. Graph-Based Refinement Results

Tab. 6 reports the results of the removal with the proposed graph-based refinement. The values between parentheses indicate the variation in performance where ‘+’ and ‘-’ signal

	FGS	GG	SAGS	GC
Counter - Tray	0.14	0.05	0.05	0.76
Counter - Plant	-	-	-	1.0
Counter - Gloves	-	0.19	-	0.81
Counter - Egg Box	-	-	-	1.0
Room - Plant	-	0.24	-	0.76
Room - Slippers	-	0.67	-	0.33
Room - Coffee Table	-	0.24	-	0.76
Kitchen - Truck	-	0.29	-	0.71
Garden - Table	0.62	0.05	-	0.33
Garden - Ball	-	-	1.0	-
Garden - Vase	-	0.14	0.10	0.76

Table 5. **User-study Votes for the best removal methods** (normalized per object). Removal performance on various objects according to the user study (the higher, the better). The users are presented with renderings after object removal from various methods and they vote for the best method on each image. For each object, we report the ratio of votes accumulated over multiple images and all users. ‘-’ indicates that no user has voted for a given method. The users often find that GaussianCut [36] is the best followed by GaussianGrouping [97] and SAGS [106].

an improvement and a deterioration respectively. The evaluation runs on Feature3DGS [106] and SAGS [33].

Failures, marked by “*”, occur when the graph can not be initialized, preventing further refinement. This is the case when the removal method being refined does not output a meaningful set of Gaussians to start from, e.g., FGS [106] does not remove the ‘Counter-eggbox’ or the ‘Room-slippers’ as indicated by their low $\text{IoU}_{\text{drop}}^{\uparrow}$ at 0.08 and 0.0. The same occurs for SAGS [33] on the ‘Counter-plant’ and the ‘Room-coffee table’. The refinement can also fail outside of this scenario, e.g., FGS [106] on the ‘Garden-table’. Still, the refinement remains relevant as one can decide to include it or not based on whether it improves the metrics. Fig. 14-17 show examples of the Gaussians removed by the refinement. These results demonstrate that the proposed graph-based refinement can improve the quality of the removal.

B.3. Metrics

Semantic IOU Evaluation. Tab. 7 presents a detailed evaluation of IoU values before and after object removal, the IoU difference ($\text{IoU}_{\text{drop}}^{\uparrow}$), and the percentage reduction from the initial IoU. These metrics are categorized by scene, removed object, and removal method. Higher $\text{IoU}_{\text{drop}}^{\uparrow}$ values, ranging from -1 to 1, indicate more effective object removal, as denoted by the \uparrow symbol.

Tab. 8 reports the ratio of images where the object remains segmented post removal. We define that an object is segmented if the semantic segmentation’s IoU is higher than a threshold. We report results on three thresholds:

User Study: Was an object removed from the image?



Figure 6. **User-study Q1: Was an object removed from this image?** Examples of images shown to the study’s users, top-bottom: yes is a correct answer (removal of the ‘Table’), no is a correct answer (no removal), and no is an incorrect answer (the ‘Plant’ is removed but the removal is not detected by users).

{0.5, 0.7, 0.9}. Figs. 18 and 19 provides examples of semantic segmentation before and after removal.

Depth difference after removal. Fig. 20 and Fig. 21 illustrate the effect of object removal on the depth map.

	IoU _{drop} ↑		acc _{Δdepth} ↑		sim _{SAM} ↓	
	FGS	SAGS	FGS	SAGS	FGS	SAGS
Plant	0.75	*	1.00	*	0.13	*
Egg Box	*	0.60 (+0.04)	*	0.98 (+0.12)	*	0.47
Plant-r	0.56 (+0.03)	0.26 (+0.09)	0.98 (+0.01)	0.37 (+0.04)	0.16 (-0.06)	0.57
Slippers	*	0.42 (+0.17)	*	0.91	*	0.45
Coffee Table	0.57	*	0.78 (+0.11)	*	0.12 (-0.14)	*
Truck	0.66 (+0.04)	*	0.96	*	0.14 (-0.21)	*
Table-g	*	0.90 (+0.09)	*	0.99 (+0.01)	*	0.04
Vase	0.9 (+0.11)	0.97 (+0.01)	1.00 (+0.01)	1.00 (+0.04)	0.00	0.11

Table 6. **Graph-based Refinement Results.** The table reports the performance of the removal after the proposed graph-based refinement on Feature3DGS [106] and SAGS [33]. Fail cases are reported with * and occur when the graph can not be initialized from the output of the removal methods.

User Study: Was an object removed from this area?



Figure 7. **User-study Q2: Was an object removed from this area?** Examples of images shown to the study’s users, top-bottom: yes is a correct answer (removal of the ‘Tray’), no is a correct answer (no removal), and no is an incorrect answer (the ‘Ball’ is removed but the removal is not detected by the users).

User Study: Image Comparison



Figure 8. **User-study Q3: Comparison of different object removal methods.** The letters at the top left corner of each image are associated with one of the evaluated methods: GaussianGrouping [97] (A), Feature3DGS [106] (B) (top row), SAGS [33] (C), and GaussianCut [36] (D) (bottom row). The images are renderings of the scene after removal. Users are asked to pick the image with the most effective object removal, *i.e.*, where the removed object is undetectable and the scene remains undisturbed. Despite similar quantitative results between GaussianGrouping [97] (A) and GaussianCut [36] (D), all users favored GaussianCut (D), demonstrating its superior visual performance in removing objects while preserving scene integrity.

User Study: Image Comparison



Figure 9. **User-study Q3: Comparison of different object removal methods.** The letters at the top left corner of each image are associated with one of the evaluated methods: GaussianGrouping [97] (A), Feature3DGS [106] (B) (top row), SAGS [33] (C), and GaussianCut [36] (D) (bottom row). The images are renderings of the scene after removal. Users are asked to select the image with the most effective object removal, where the removed object is undetectable and the scene remains undisturbed. Interestingly, all users favored SAGS (C), even though it did not achieve the best quantitative results, highlighting the importance of subjective evaluation in assessing visual quality.

User Study: Image Comparison

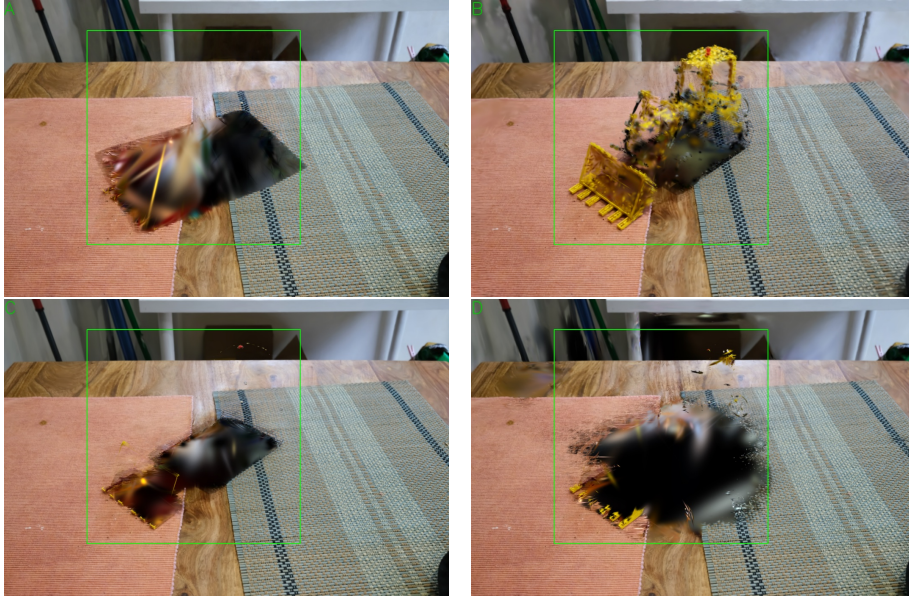


Figure 10. **User-study Q3: Comparison of different object removal methods.** The letters at the top left corner of each image are associated with one of the evaluated methods: GaussianGrouping [97] (A), Feature3DGS [106] (B) (top row), SAGS [33] (C), and GaussianCut [36] (D) (bottom row). The images are renderings of the scene after removal. Users are asked to select the image with the most effective object removal, where the removed object is undetectable and the scene remains undisturbed. Despite similar quantitative results between SAGS (C) and GaussianCut (D), all users favored SAGS (C), demonstrating its superior visual performance in seamlessly removing objects while preserving scene integrity.

User Study: Image Comparison

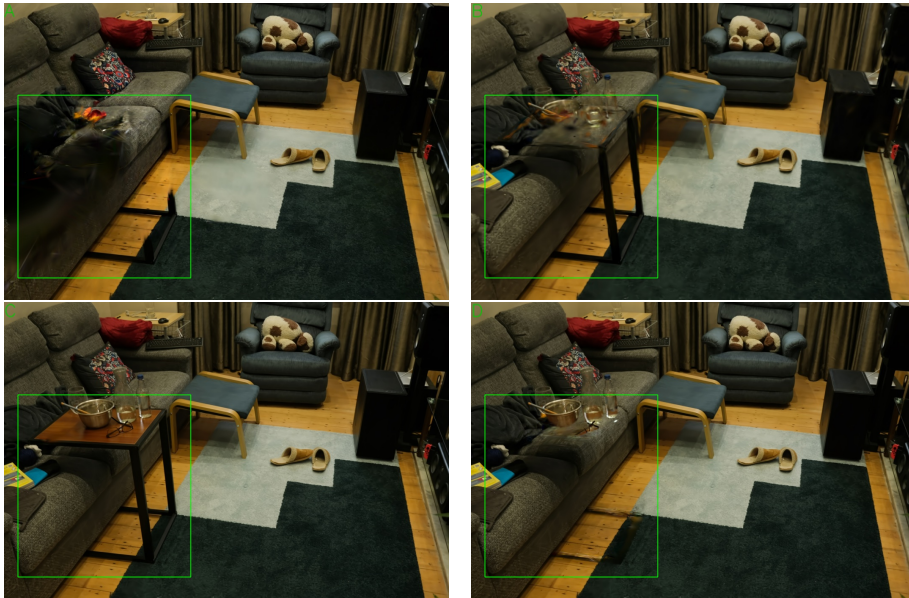


Figure 11. **User-study Q3: Comparison of different object removal methods.** The letters at the top left corner of each image are associated with one of the evaluated methods: GaussianGrouping [97] (A), Feature3DGS [106] (B) (top row), SAGS [33] (C), and GaussianCut [36] (D) (bottom row). The images are renderings of the scene after removal. Users are asked to select the image with the most effective object removal, where the removed object is undetectable and the scene remains undisturbed. Despite similar quantitative results between GaussianGrouping (A) and GaussianCut (D), all users favored GaussianCut (D), highlighting its superior visual performance in removing objects while preserving scene integrity.

User Study: Image Comparison

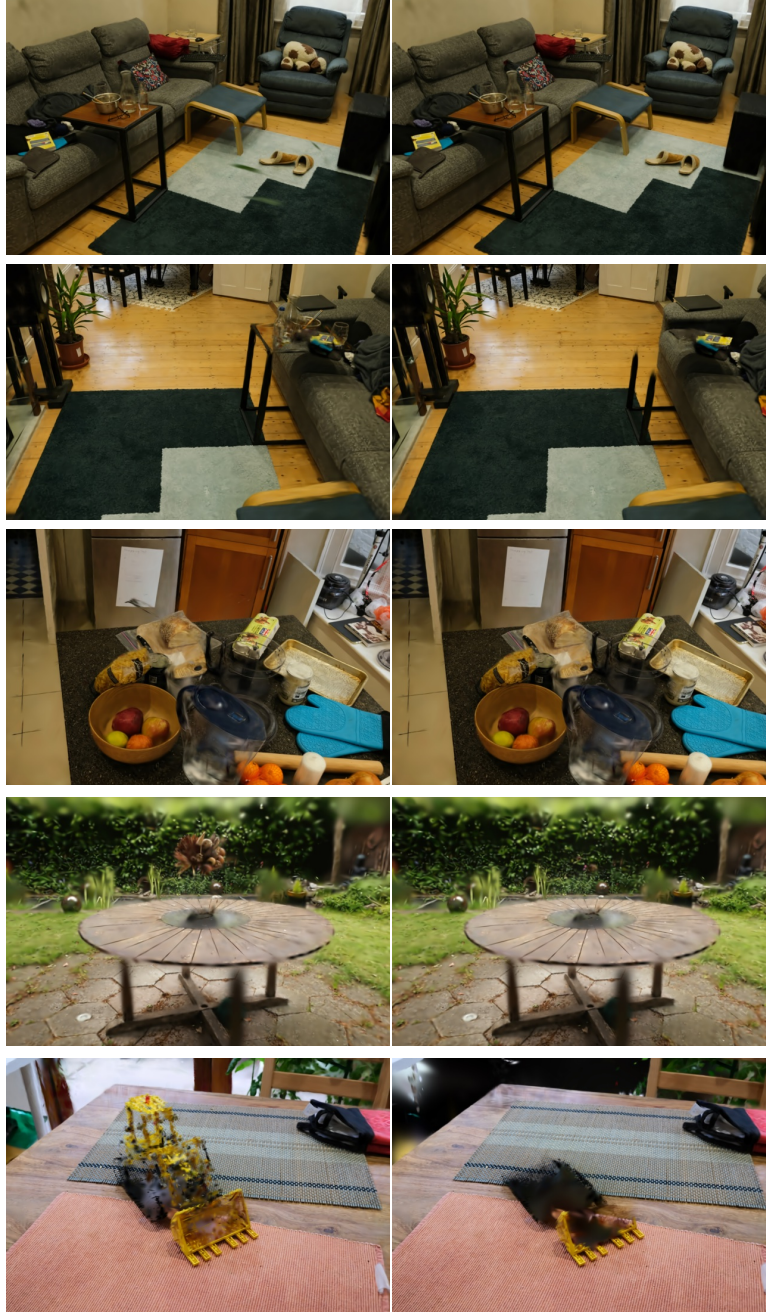


Figure 12. **User-study Q4: Graph-based refinement on Feature3DGS [106].** Left-Right: before refinement, after refinement. All users prefer the refined removal, indicating that the proposed graph-based refinement improves the visual quality of object removal.

User Study: Image Comparison

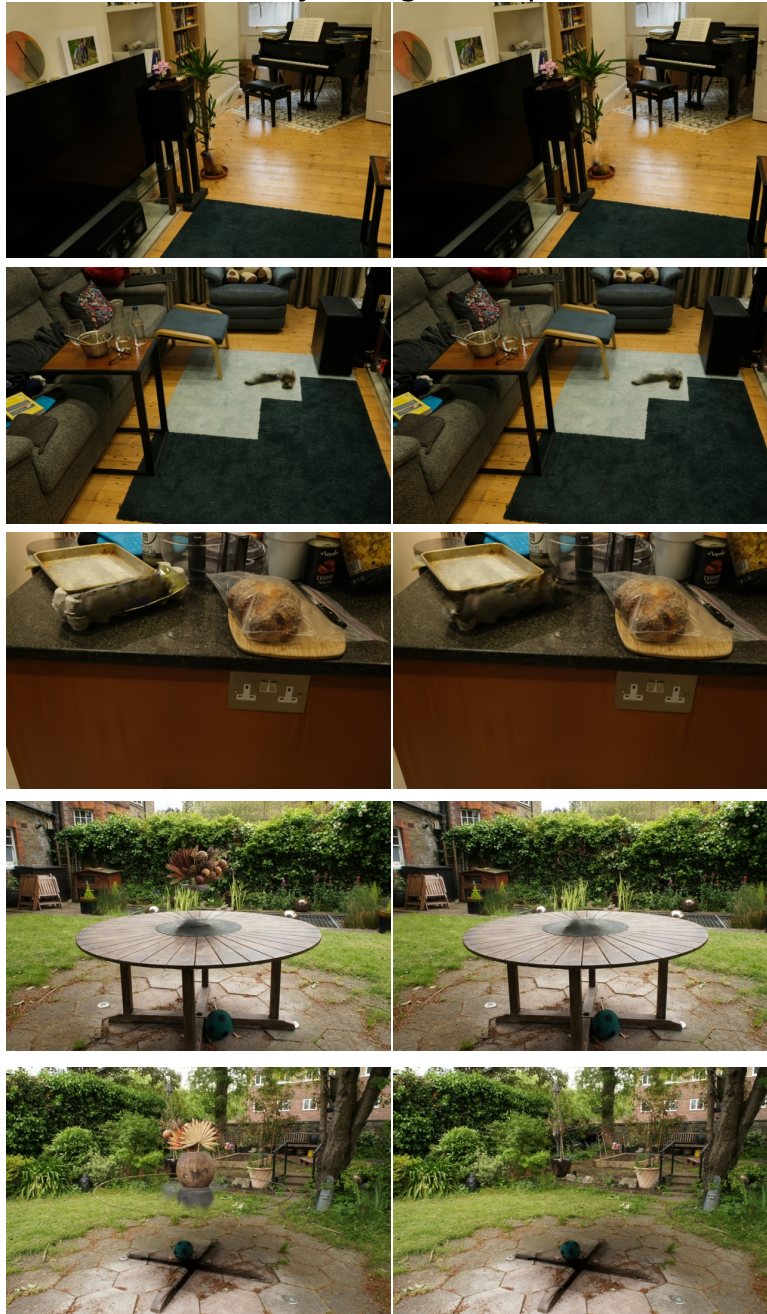


Figure 13. **User-study Q4: Graph-based refinement on SAGS [33]**. Left-Right: before refinement, after refinement. All users prefer the refined removal, indicating that the proposed graph-based refinement improves the visual quality of object removal.

GraphCut applied after Feature 3DGS

Suggested Gaussians for Further Removal by GraphCut

Rendered Image After Removal



Figure 14. **Graph-based refinement of the removal on Feature3DGS [106].** Left: the image shows the rendering after removal and before refinement. The Gaussians to be removed by the refinement are colored in pink. Right: the images are rendered after the refined removal. The improved removal of the ‘Table’ in the right image demonstrates the effectiveness of the proposed graph-based refinement in identifying and eliminating residual parts left by the initial method.

GraphCut applied after Feature 3DGS

Suggested Gaussians for Further Removal by GraphCut

Rendered Image After Removal

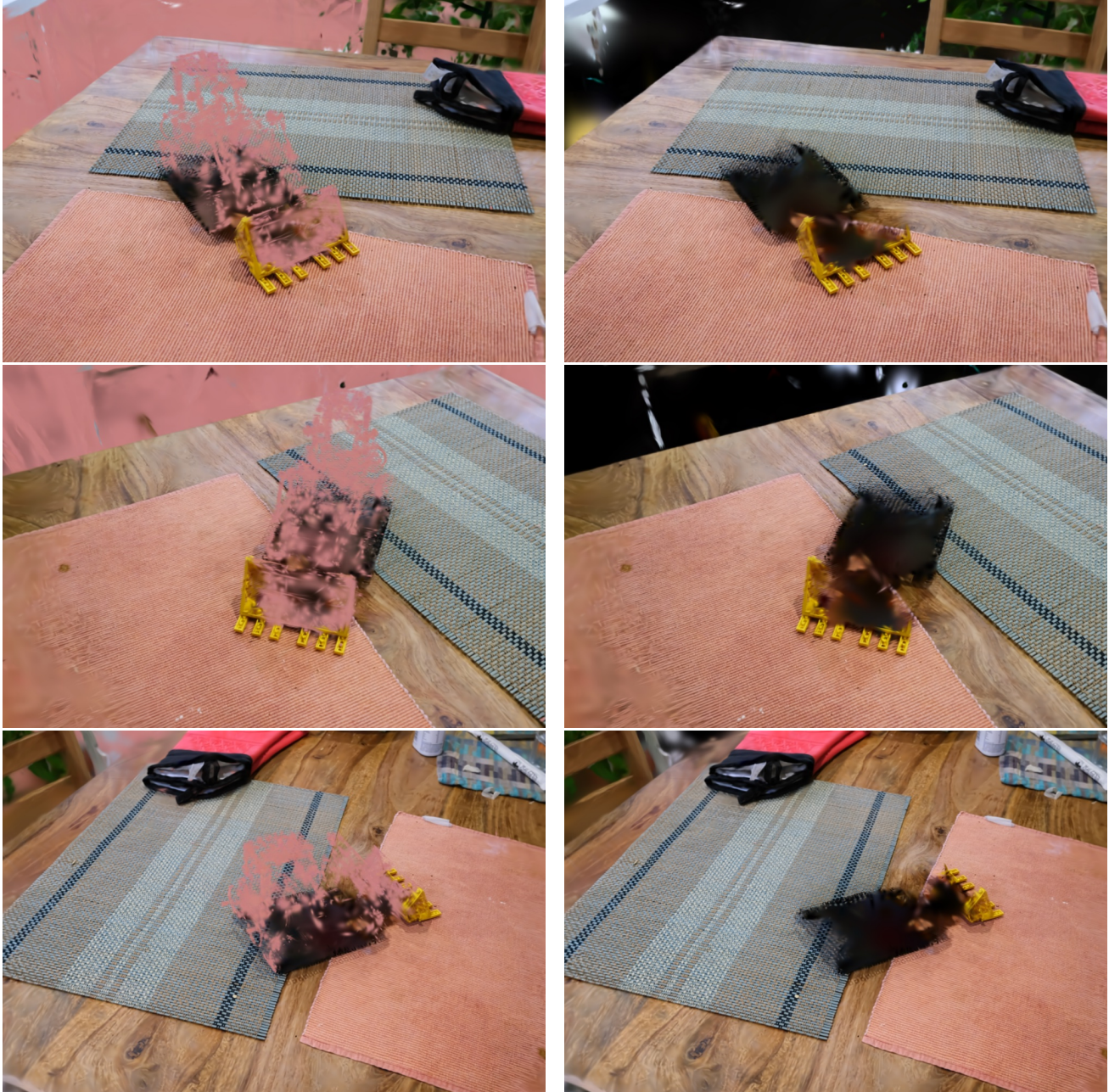


Figure 15. **Graph-based refinement of the removal on Feature3DGS [106]**. Left: the image shows the rendering after removal and before refinement. The Gaussians to be removed by the refinement are colored in pink. Right: the images are rendered after the refined removal. The improved removal of the ‘Truck’ in the right image demonstrates the effectiveness of the proposed graph-based refinement in identifying and eliminating residual parts left by the initial method.

GraphCut applied after SAGS

Suggested Gaussians for Further Removal by GraphCut

Rendered Image After Removal

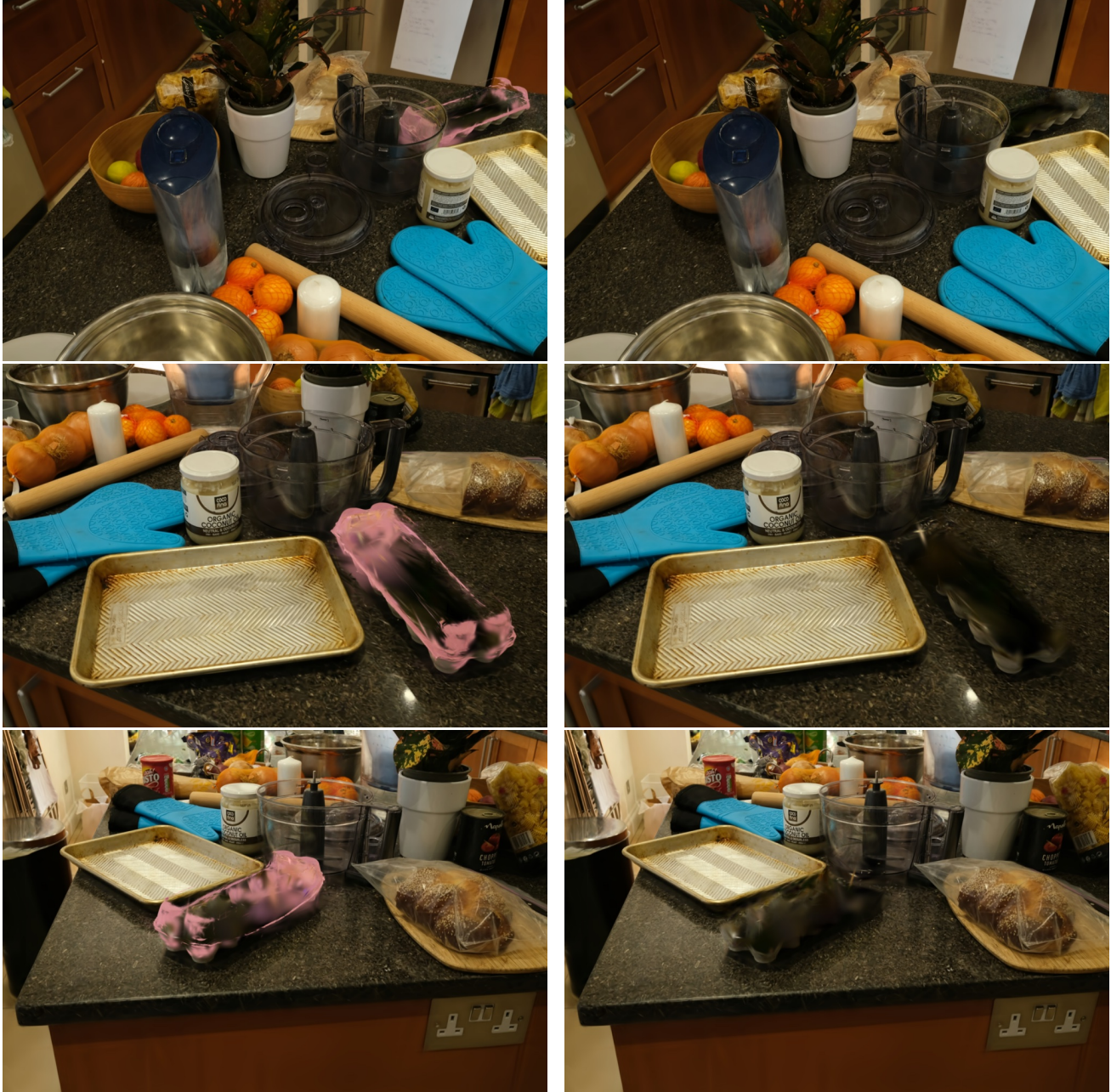


Figure 16. **Graph-based refinement of the removal on SAGS [33]**. Left: the image shows the rendering after removal and before refinement. The Gaussians to be removed by the refinement are colored in pink. Right: the images are rendered after the refined removal. The improved removal of the 'Egg-box' in the right image demonstrates the effectiveness of the proposed graph-based refinement in identifying and eliminating residual parts left by the initial method.

GraphCut applied after SAGS

Suggested Gaussians for Further Removal by GraphCut

Rendered Image After Removal

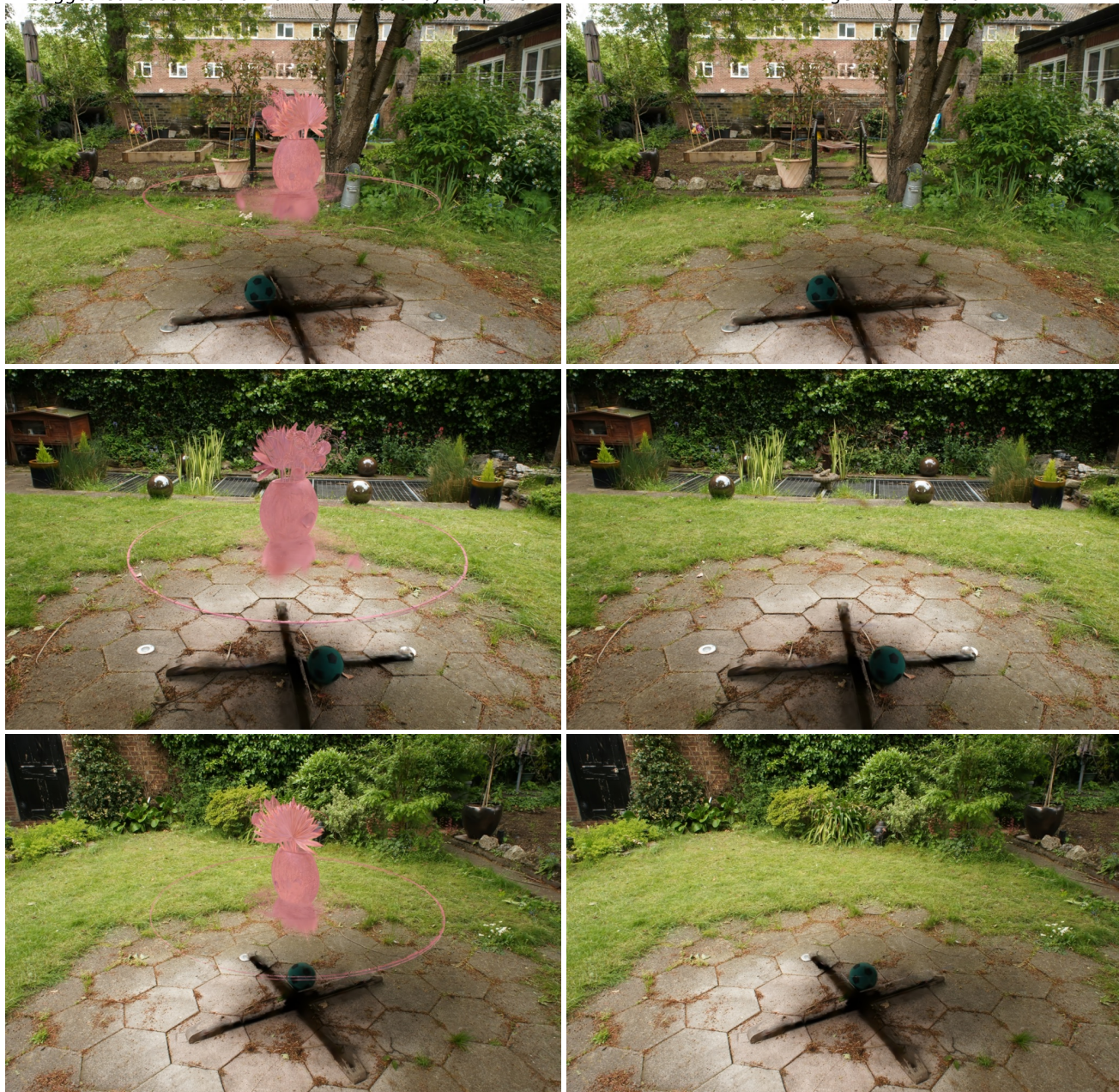


Figure 17. **Graph-based refinement of the removal on SAGS [33].** Left: the image shows the rendering after removal and before refinement. The Gaussians to be removed by the refinement are colored in pink. Right: the images are rendered after the refined removal. The improved removal of the 'Table' in the right image demonstrates the effectiveness of the proposed graph-based refinement in identifying and eliminating residual parts left by the initial method.

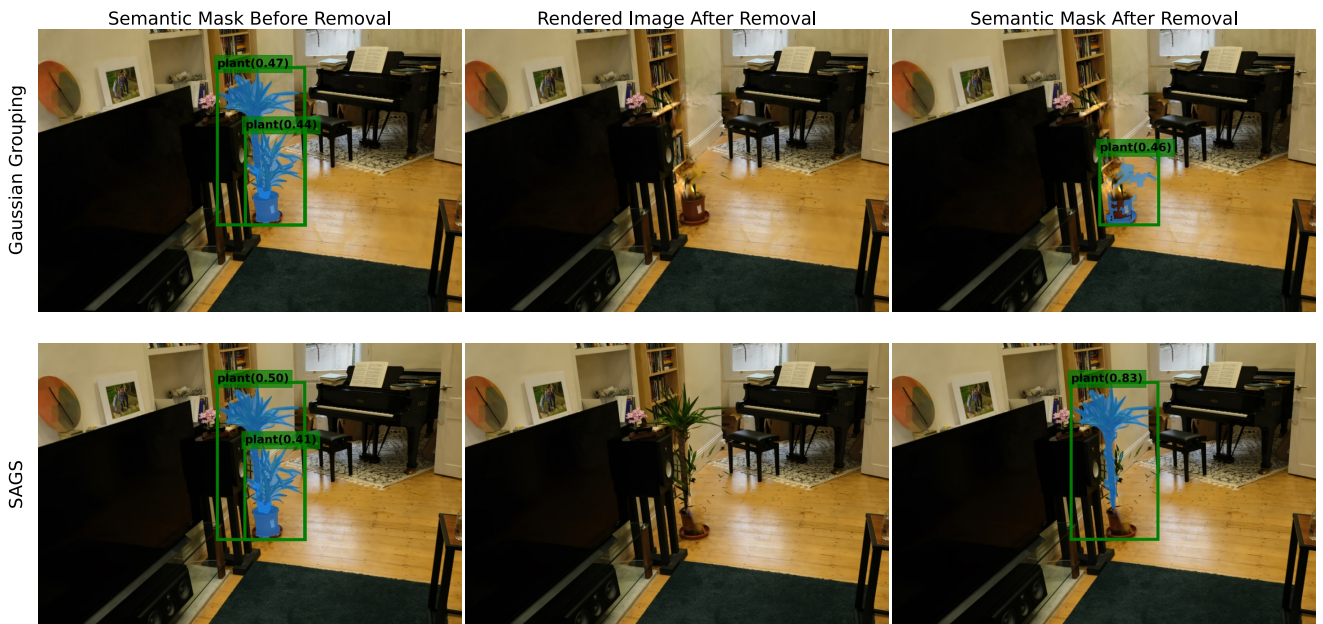


Figure 18. **GroundedSAM [39, 54, 77] Semantic Segmentation Examples** on renderings from GaussianGrouping [97] and SAGS [33]. The left image shows the rendering before removal with its corresponding segmentation. The middle image presents the rendered scene after removal and the right image shows the segmentation after removal. Even after removal, GroundedSAM still segments the ‘Plant’, which indicates that the object or parts of the object remain in the scene.

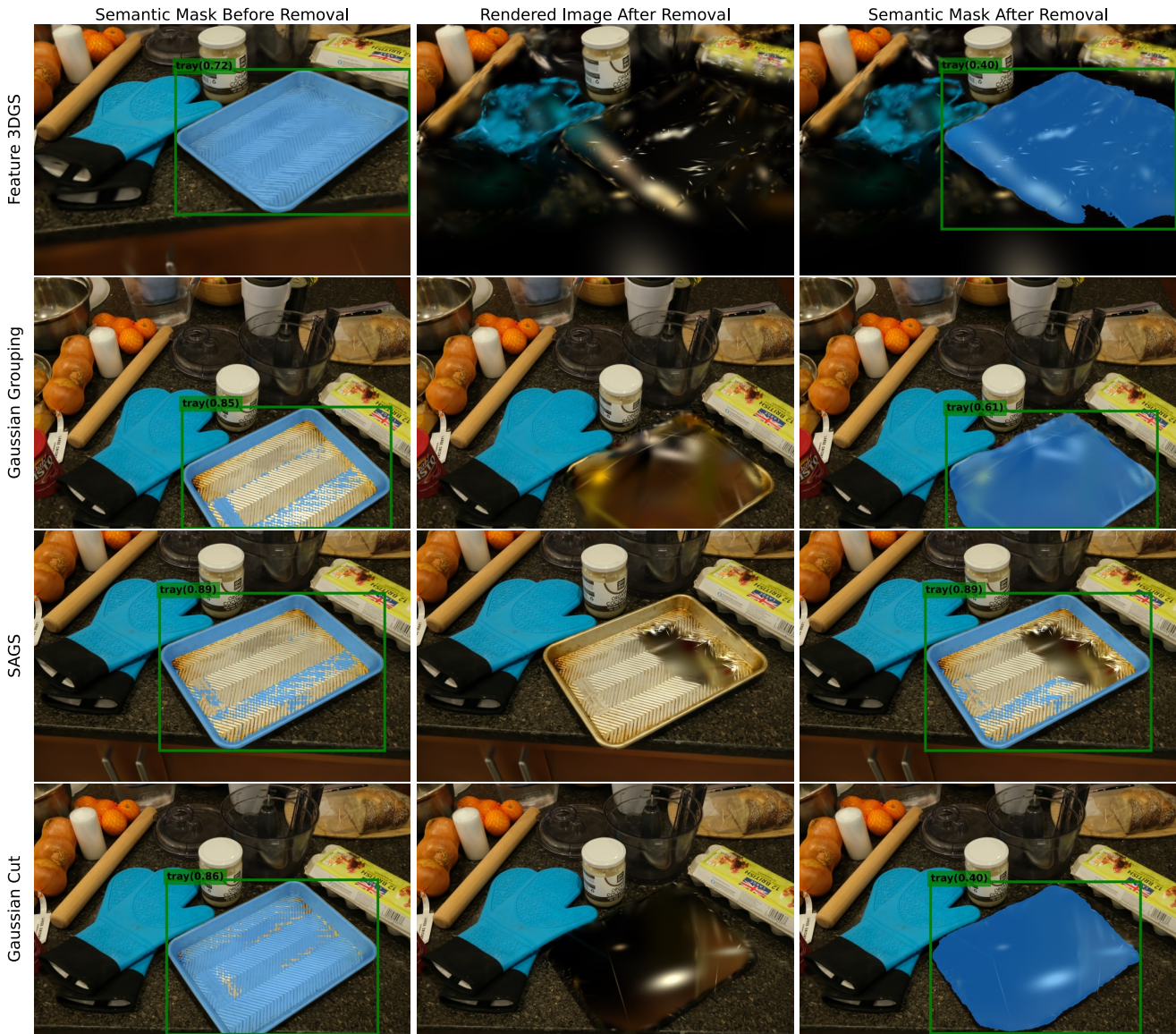


Figure 19. **GroundedSAM** [39, 54, 77] **Semantic Segmentation Examples** on renderings from Feature3DGS [106], GaussianGrouping [97], SAGS [33], and GaussianCut [36]. The left image shows the rendering before removal with its corresponding segmentation. The middle image presents the rendered scene after removal and the right image shows the segmentation after removal. Even after removal, GroundedSAM still segments the ‘Tray’, which indicates either that the object or parts of the object remain in the scene (SAGS) or that there remains invisible information about the object that the segmentation can detect (Feature3DGS, GaussianGrouping, GaussianCut).

Scene	Object	Method	$mIoU_{pre}$	$mIoU_{post}$	IoU_{drop}^{\uparrow}	
Counter	Baking Tray	Gaussian Grouping	0.61	0.08	<u>0.53 / 86.9</u>	
		Feature 3DGS	0.54	0.21	0.34 / 63.0	
		SAGS	0.62	0.52	0.10 / 16.1	
		Gaussian Cut	0.63	0.01	0.62 / 98.4	
	Plant	Gaussian Grouping	0.84	0.00	<u>0.84 / 100</u>	
		Feature 3DGS	0.75	0.00	0.75 / 100	
		SAGS	0.85	0.82	0.03 / 3.50	
		Gaussian Cut	0.86	0.00	0.86 / 100	
	Blue Gloves	Gaussian Grouping	0.75	0.15	0.60 / 80.0	
		Feature 3DGS	0.67	0.66	0.01 / 1.50	
		SAGS	0.74	0.64	0.10 / 13.5	
		Gaussian Cut	0.74	0.15	0.60 / 81.1	
	Egg Box	Gaussian Grouping	0.63	0.00	0.63 / 100	
		Feature 3DGS	0.78	0.7	0.08 / 10.3	
		SAGS	0.6	0.04	0.56 / 93.3	
		Gaussian Cut	0.63	0.01	<u>0.62 / 98.4</u>	
Room	Plant	Gaussian Grouping	0.50	0.23	0.26 / 13.0	
		Feature 3DGS	0.53	0.00	0.53 / 100	
		SAGS	0.52	0.35	0.17 / 32.7	
		Gaussian Cut	0.53	0.00	0.53 / 100	
	Slippers	Gaussian Grouping	0.96	0.14	0.82 / 85.4	
		Feature 3DGS	0.96	0.96	0.00 / 0.00	
		SAGS	0.96	0.71	0.25 / 26.0	
		Gaussian Cut	0.97	0.48	<u>0.48 / 49.5</u>	
	Coffee Table	Gaussian Grouping	0.88	0.02	0.86 / 97.7	
		Feature 3DGS	0.86	0.29	0.57 / 66.3	
		SAGS	0.89	0.89	0.00 / 0.00	
		Gaussian Cut	0.89	0.03	0.86 / 96.6	
	Kitchen	Truck	Gaussian Grouping	0.67	0.06	0.61 / 91.0
			Feature 3DGS	0.67	0.05	0.62 / 92.5
			SAGS	0.67	0.00	0.67 / 100
			Gaussian Cut	0.67	0.01	<u>0.66 / 98.5</u>
Garden	Table	Gaussian Grouping	0.89	0.41	0.48 / 42.7	
		Feature 3DGS	0.90	0.24	0.67 / 74.4	
		SAGS	0.90	0.09	<u>0.81 / 90.0</u>	
		Gaussian Cut	0.90	0.04	0.86 / 95.6	
	Ball	Gaussian Grouping	0.16	0.00	0.16 / 100	
		Feature 3DGS	0.06	0.06	0.00 / 0.00	
		SAGS	0.41	0.0	<u>0.41 / 100</u>	
		Gaussian Cut	0.42	0.00	0.42 / 100	
	Vase	Gaussian Grouping	0.85	0.22	0.64 / 75.3	
		Feature 3DGS	0.90	0.11	0.79 / 87.8	
		SAGS	0.97	0.01	<u>0.96 / 99.0</u>	
		Gaussian Cut	0.97	0.01	0.97 / 100	

Table 7. **Breakdown of the proposed semantic segmentation IoU_{drop}^{\uparrow} metric.** $IoU_{drop} = IoU_{post} - IoU_{pre}$ and the higher, the better the removal. The best-performing method is highlighted in bold and the second-best is underlined. We also report the individual segmentation IoUs before and after removal, IoU_{pre} and IoU_{post} respectively.

Scene	Object	Method	$\text{acc}_{\text{IoU-post}>0.5} \downarrow$	$\text{acc}_{\text{IoU-post}>0.7} \downarrow$	$\text{acc}_{\text{IoU-post}>0.9} \downarrow$
Counter	Baking Tray	Gaussian Grouping	8.50	8.50	5.70
		Feature 3DGS	21.7	19.8	17.9
		SAGS	51.9	44.3	30.2
		Gaussian Cut	0.09	0.09	0.09
	Plant	Gaussian Grouping	0.00	0.00	0.00
		Feature 3DGS	0.00	0.00	0.00
		SAGS	83.3	83.3	83.3
		Gaussian Cut	0.00	0.00	0.00
	Blue Gloves	Gaussian Grouping	16.3	16.3	9.60
		Feature 3DGS	72.1	66.3	52.9
		SAGS	66.3	50.0	44.2
		Gaussian Cut	17.3	17.3	3.8
Egg Box	Gaussian Grouping	0.00	0.00	0.00	
	Feature 3DGS	80.4	79.4	71.0	
	SAGS	4.10	4.10	3.10	
	Gaussian Cut	1.00	0.00	0.00	
Room	Plant	Gaussian Grouping	20.0	12.0	8.00
		Feature 3DGS	0.00	0.00	0.00
		SAGS	28.0	20.0	8.0%
		Gaussian Cut	0.00	0.00	0.00
	Slippers	Gaussian Grouping	14.7	14.7	13.2
		Feature 3DGS	98.5	98.6	98.5
		SAGS	72.1	67.6	22.1
		Gaussian Cut	55.9	41.2	16.2
	Coffee Table	Gaussian Grouping	1.00	1.00	1.00
		Feature 3DGS	38.4	21.2	5.10
		SAGS	90.9	89.9	89.9
		Gaussian Cut	1.00	1.00	1.00
Kitchen	Truck	Gaussian Grouping	7.80	1.50	0.00
		Feature 3DGS	4.90	4.90	4.40
		SAGS	0.00	0.00	0.00
		Gaussian Cut	0.05	0.00	0.00
Garden	Table	Gaussian Grouping	45.9	29.0	10.0
		Feature 3DGS	29.7	18.2	0.00
		SAGS	12.2	7.40	0.00
		Gaussian Cut	4.70	3.30	0.00
	Ball	Gaussian Grouping	0.00	0.00	0.00
		Feature 3DGS	6.10	6.10	6.10
		SAGS	0.00	0.00	0.00
		Gaussian Cut	0.00	0.00	0.00
	Vase	Gaussian Grouping	21.6	20.2	19.6
		Feature 3DGS	10.8	9.50	7.40
		SAGS	0.00	0.00	0.00
		Gaussian Cut	0.00	0.00	0.00

Table 8. **Additional evaluation based on how well the object is segmented after removal.** This table presents the ratio of images where the object is still segmented even after removal. We define that the object is segmented if the semantic segmentation IoU is higher than a threshold. We report the results for the thresholds $\{0.5, 0.7, \text{ and } 0.9\}$.

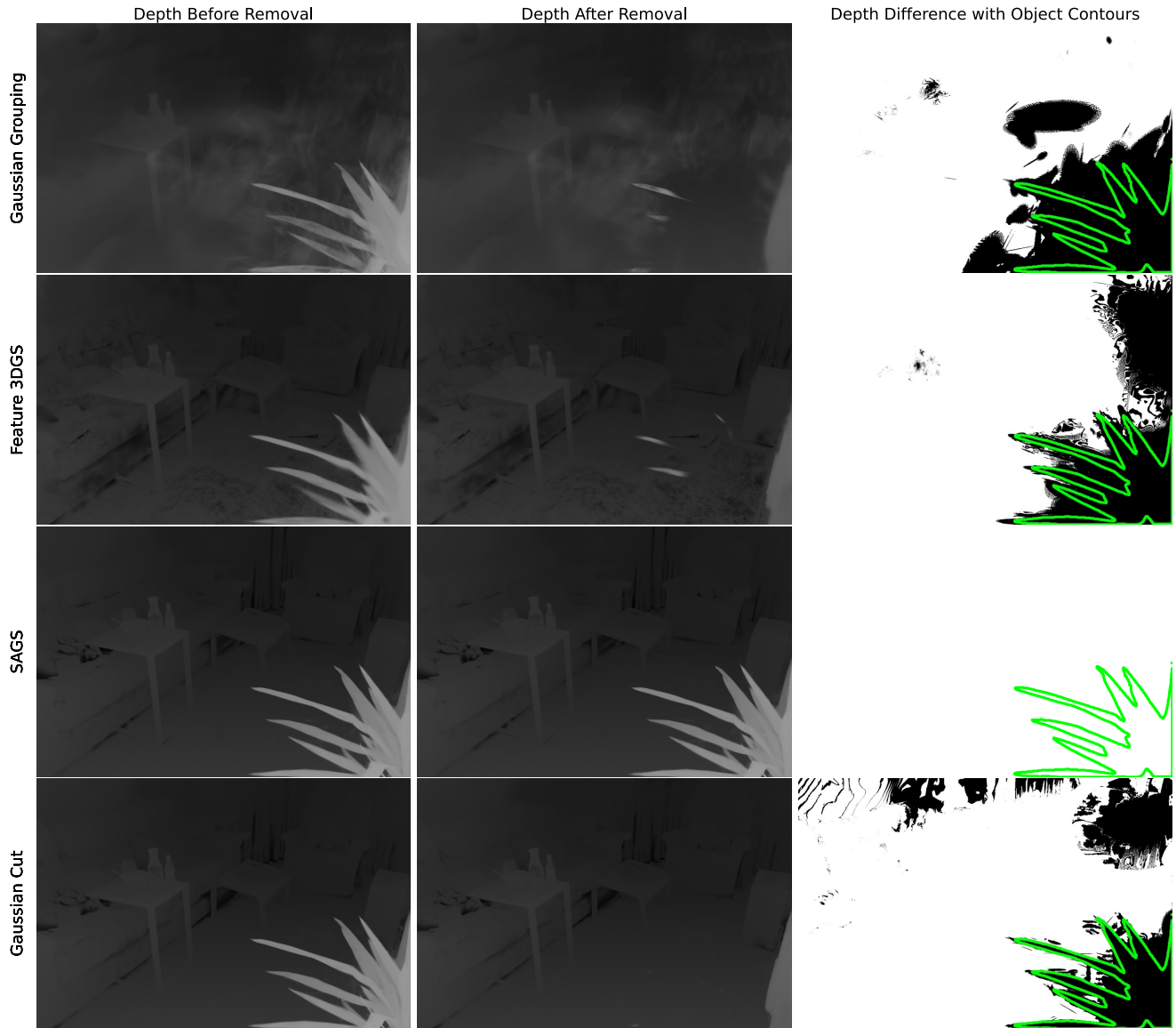


Figure 20. **Depth rendering before and after object removal** on Feature3DGS [106], GaussianGrouping [97], SAGS [33], and GaussianCut [36]. Left-Right: the original depth map, depth after removal, and the difference map highlighting the removed object’s contours. Notably, SAGS [33] did not capture any depth difference. While other methods exhibit depth changes (black region in the right image), the changes do not overlay with the pseudo-ground-truth object mask (green outline), which suggests that the removal is subpar.

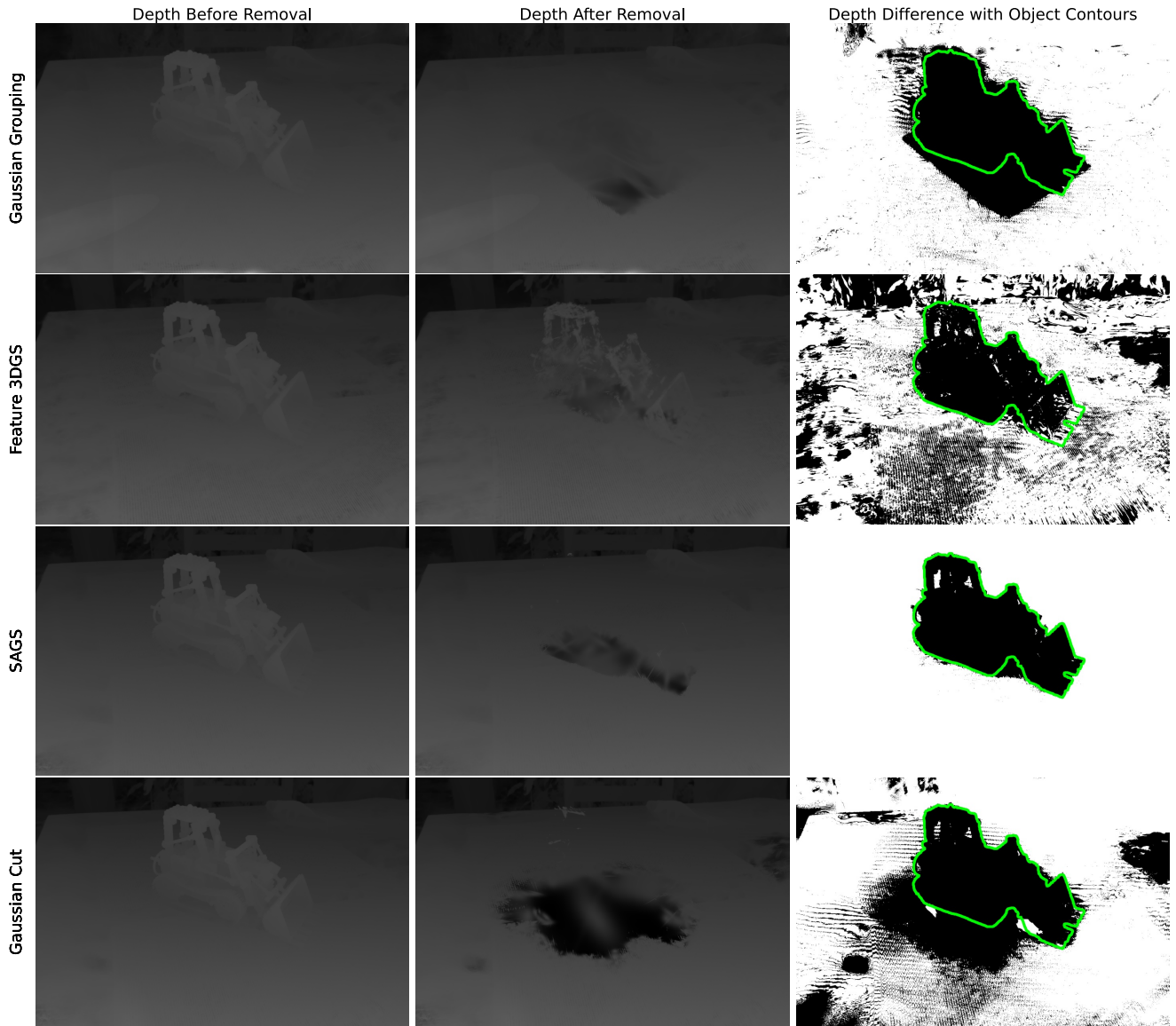


Figure 21. **Depth rendering before and after object removal** on Feature3DGS [106], GaussianGrouping [97], SAGS [33], and GaussianCut [36]. Left-Right: the original depth map, depth after removal, and the difference map highlighting the removed object’s contours. SAGS achieves the best removal as measured by the depth differences that overlay well with the pseudo-ground-truth object mask (green outline). In contrast, other methods induce depth changes beyond the object’s boundaries, which indicates unintended modifications of the scene’s representation.

References

- [1] Accelerating AR and AI from a human perspective. <https://www.projectaria.com/>. 3
- [2] Luma AI Interactive Scenes. <https://lumalabs.ai/interactive-scenes>. 1
- [3] Polycam. <https://poly.cam/spatial-capture>. 1
- [4] Postshot. <https://www.jawset.com/>. 1
- [5] Realityscan - 3d scanning app. 1
- [6] Scaniverse. niantic, inc. <https://scaniverse.com/>. 1
- [7] Spectacles, AR glasses powered by Snap OS. <https://www.spectacles.com/>. 3
- [8] Xreal One, AR for All. <https://www.xreal.com/>. 3
- [9] Josh Achiam, Steven Adler, Sandhini Agarwal, Lama Ahmad, Ilge Akkaya, Florencia Leoni Aleman, Diogo Almeida, Janko Altenschmidt, Sam Altman, Shyamal Anadkat, et al. Gpt-4 technical report. *arXiv preprint arXiv:2303.08774*, 2023. 1, 3
- [10] Aikaterini Adam, Torsten Sattler, Konstantinos Karantzas, and Tomas Pajdla. Objects can move: 3d change detection by geometric transformation consistency. In *European Conference on Computer Vision*, pages 108–124. Springer, 2022. 5
- [11] Aikaterini Adam, Konstantinos Karantzas, Lazaros Grammatikopoulos, and Torsten Sattler. Has anything changed? 3d change detection by 2d segmentation masks. *arXiv preprint arXiv:2312.01148*, 2023. 5
- [12] Vijay Badrinarayanan, Alex Kendall, and Roberto Cipolla. Segnet: A deep convolutional encoder-decoder architecture for image segmentation. *IEEE transactions on pattern analysis and machine intelligence*, 39(12):2481–2495, 2017. 3
- [13] Jonathan T. Barron. A generalization of otsu’s method and minimum error thresholding. In *European conference on computer vision*, 2020. 5
- [14] Jonathan T Barron, Ben Mildenhall, Dor Verbin, Pratul P Srinivasan, and Peter Hedman. Mip-nerf 360: Unbounded anti-aliased neural radiance fields. In *Proceedings of the IEEE/CVF conference on computer vision and pattern recognition*, pages 5470–5479, 2022. 1, 2, 6, 11
- [15] Yash Bhalgat, Iro Laina, João F Henriques, Andrea Vedaldi, and Andrew Zisserman. Contrastive lift: 3d object instance segmentation by slow-fast contrastive fusion. *Advances in Neural Information Processing Systems*, 36, 2024. 3
- [16] Yuri Boykov, Olga Veksler, and Ramin Zabih. Fast approximate energy minimization via graph cuts. *IEEE Transactions on pattern analysis and machine intelligence*, 23(11):1222–1239, 2001. 5
- [17] Tim Brooks, Bill Peebles, Connor Holmes, Will DePue, Yufei Guo, Li Jing, David Schnurr, Joe Taylor, Troy Luhman, Eric Luhman, et al. Video generation models as world simulators. *OpenAI Blog*, 1:8, 2024. 3
- [18] Mathilde Caron, Hugo Touvron, Ishan Misra, Hervé Jégou, Julien Mairal, Piotr Bojanowski, and Armand Joulin. Emerging properties in self-supervised vision transformers. In *Proceedings of the IEEE/CVF international conference on computer vision*, pages 9650–9660, 2021. 3
- [19] Jiazhong Cen, Jiemin Fang, Chen Yang, Lingxi Xie, Xiaopeng Zhang, Wei Shen, and Qi Tian. Segment any 3d gaussians. *arXiv preprint arXiv:2312.00860*, 2023. 1, 3
- [20] Jiazhong Cen, Zanwei Zhou, Jiemin Fang, Wei Shen, Lingxi Xie, Dongsheng Jiang, Xiaopeng Zhang, Qi Tian, et al. Segment anything in 3d with nerfs. *Advances in Neural Information Processing Systems*, 36:25971–25990, 2023. 3
- [21] Kunal Chelani, Torsten Sattler, Fredrik Kahl, and Zuzana Kukelova. Privacy-preserving representations are not enough: Recovering scene content from camera poses. In *Proceedings of the IEEE/CVF Conference on Computer Vision and Pattern Recognition*, pages 13132–13141, 2023. 3
- [22] Anpei Chen, Haofei Xu, Stefano Esposito, Siyu Tang, and Andreas Geiger. Lara: Efficient large-baseline radiance fields. In *European Conference on Computer Vision*, pages 338–355. Springer, 2024. 1, 2
- [23] Liang-Chieh Chen, George Papandreou, Iasonas Kokkinos, Kevin Murphy, and Alan L Yuille. Deeplab: Semantic image segmentation with deep convolutional nets, atrous convolution, and fully connected crfs. *IEEE transactions on pattern analysis and machine intelligence*, 40(4):834–848, 2017. 3
- [24] Minghao Chen, Iro Laina, and Andrea Vedaldi. Dge: Direct gaussian 3d editing by consistent multi-view editing. In *European Conference on Computer Vision*, pages 74–92. Springer, 2024. 1
- [25] Yuedong Chen, Haofei Xu, Chuanxia Zheng, Bohan Zhuang, Marc Pollefeys, Andreas Geiger, Tat-Jen Cham, and Jianfei Cai. Mvsplat: Efficient 3d gaussian splatting from sparse multi-view images. In *European Conference on Computer Vision*, pages 370–386. Springer, 2024. 1, 2
- [26] Seokhun Choi, Hyeonseop Song, Jaechul Kim, Taehyeong Kim, and Hoseok Do. Click-gaussian: Interactive segmentation to any 3d gaussians. In *European Conference on Computer Vision*, pages 289–305. Springer, 2024. 1
- [27] Seokhun Choi, Hyeonseop Song, Jaechul Kim, Taehyeong Kim, and Hoseok Do. Click-gaussian: Interactive segmentation to any 3d gaussians. In *European Conference on Computer Vision*, pages 289–305. Springer, 2024. 1, 3
- [28] Yasutaka Furukawa and Jean Ponce. Accurate, dense, and robust multiview stereopsis. *IEEE transactions on pattern analysis and machine intelligence*, 32(8):1362–1376, 2009. 2
- [29] Benjamin Graham and Laurens Van der Maaten. Submanifold sparse convolutional networks. *arXiv preprint arXiv:1706.01307*, 2017. 3
- [30] Dorothy M Greig, Bruce T Porteous, and Allan H Seheult. Exact maximum a posteriori estimation for binary images. *Journal of the Royal Statistical Society Series B: Statistical Methodology*, 51(2):271–279, 1989. 5
- [31] Michael M Grynbaum and Ryan Mac. The times sues openai and microsoft over ai use of copyrighted work. *The New York Times*, 27, 2023. 3
- [32] Qiao Gu, Zhaoyang Lv, Duncan Frost, Simon Green, Julian Straub, and Chris Sweeney. Egolifter: Open-world 3d seg-

- mentation for egocentric perception. In *European Conference on Computer Vision*, pages 382–400. Springer, 2024. 1, 3
- [33] Xu Hu, Yuxi Wang, Lue Fan, Junsong Fan, Junran Peng, Zhen Lei, Qing Li, and Zhaoxiang Zhang. Semantic anything in 3d gaussians. *arXiv e-prints*, pages arXiv–2401, 2024. 1, 6, 7, 8, 9, 11, 12, 13, 14, 15, 16, 18, 21, 22, 23, 24, 27, 28
- [34] Rui Huang, Songyou Peng, Ayca Takmaz, Federico Tombari, Marc Pollefeys, Shiji Song, Gao Huang, and Francis Engelmann. Segment3d: Learning fine-grained class-agnostic 3d segmentation without manual labels. In *European Conference on Computer Vision*, pages 278–295. Springer, 2024. 1, 2
- [35] Erin Illman and Paul Temple. California consumer privacy act. *The Business Lawyer*, 75(1):1637–1646, 2019. 3, 9
- [36] Umangi Jain, Ashkan Mirzaei, and Igor Gilitschenski. Gaussiancut: Interactive segmentation via graph cut for 3d gaussian splatting. In *The Thirty-eighth Annual Conference on Neural Information Processing Systems*, 2024. 1, 3, 5, 6, 7, 9, 11, 12, 13, 15, 16, 24, 27, 28
- [37] Bernhard Kerbl, Georgios Kopanas, Thomas Leimkühler, and George Drettakis. 3d gaussian splatting for real-time radiance field rendering. *ACM Transactions on Graphics*, 42(4), 2023. 1, 2, 3, 6, 11
- [38] Justin Kerr, Chung Min Kim, Ken Goldberg, Angjoo Kanazawa, and Matthew Tancik. Lrf: Language embedded radiance fields. In *Proceedings of the IEEE/CVF International Conference on Computer Vision*, pages 19729–19739, 2023. 1, 3
- [39] Alexander Kirillov, Eric Mintun, Nikhila Ravi, Hanzi Mao, Chloe Rolland, Laura Gustafson, Tete Xiao, Spencer Whitehead, Alexander C. Berg, Wan-Yen Lo, Piotr Dollár, and Ross Girshick. Segment anything. *arXiv:2304.02643*, 2023. 2, 3, 4, 6, 7, 9, 11, 23, 24
- [40] Sosuke Kobayashi, Eiichi Matsumoto, and Vincent Sitzmann. Decomposing nerf for editing via feature field distillation. *Advances in neural information processing systems*, 35:23311–23330, 2022. 3
- [41] Sebastian Koch, Johanna Wald, Mirco Colosi, Narunas Vaskevicius, Pedro Hermosilla, Federico Tombari, and Timo Ropinski. Relationfield: Relate anything in radiance fields. *arXiv preprint arXiv:2412.13652*, 2024. 1
- [42] Jonas Kulhanek and Torsten Sattler. Tetra-nerf: Representing neural radiance fields using tetrahedra. In *Proceedings of the IEEE/CVF International Conference on Computer Vision*, pages 18458–18469, 2023. 1, 2
- [43] Jonas Kulhanek, Songyou Peng, Zuzana Kukelova, Marc Pollefeys, and Torsten Sattler. Wildgaussians: 3d gaussian splatting in the wild. In *The Thirty-Eighth Annual Conference on Neural Information Processing Systems (NeurIPS 2024)*, 2024. 1, 2
- [44] Abhijit Kundu, Xiaoqi Yin, Alireza Fathi, David Ross, Brian Brewington, Thomas Funkhouser, and Caroline Pantofaru. Virtual multi-view fusion for 3d semantic segmentation. In *Computer Vision–ECCV 2020: 16th European Conference, Glasgow, UK, August 23–28, 2020, Proceedings, Part XXIV 16*, pages 518–535. Springer, 2020. 2
- [45] Svetlana Lazebnik, Edmond Boyer, and Jean Ponce. On computing exact visual hulls of solids bounded by smooth surfaces. In *Proceedings of the 2001 IEEE Computer Society Conference on Computer Vision and Pattern Recognition. CVPR 2001*, pages I–I. IEEE, 2001. 2
- [46] Boyi Li, Kilian Q Weinberger, Serge Belongie, Vladlen Koltun, and Rene Ranftl. Language-driven semantic segmentation. In *International Conference on Learning Representations*, 2022. 3, 6
- [47] Feng Li, Hao Zhang, Peize Sun, Xueyan Zou, Shilong Liu, Chunyuan Li, Jianwei Yang, Lei Zhang, and Jianfeng Gao. Segment and recognize anything at any granularity. In *European Conference on Computer Vision*, pages 467–484. Springer, 2024. 3, 6
- [48] Siyun Liang, Sen Wang, Kunyi Li, Michael Niemeyer, Stefano Gasperini, Nassir Navab, and Federico Tombari. Superseg: Open-vocabulary 3d segmentation with structured super-gaussians. *arXiv preprint arXiv:2412.10231*, 2024. 1
- [49] Guibiao Liao, Jiankun Li, Zhenyu Bao, Xiaoqing Ye, Jingdong Wang, Qing Li, and Kanglin Liu. Clip-gs: Clip-informed gaussian splatting for real-time and view-consistent 3d semantic understanding. *arXiv preprint arXiv:2404.14249*, 2024. 3
- [50] Jiaqi Lin, Zhihao Li, Xiao Tang, Jianzhuang Liu, Shiyong Liu, Jiayue Liu, Yangdi Lu, Xiaofei Wu, Songcen Xu, Youliang Yan, et al. Vastgaussian: Vast 3d gaussians for large scene reconstruction. In *Proceedings of the IEEE/CVF Conference on Computer Vision and Pattern Recognition*, pages 5166–5175, 2024. 1, 2
- [51] Dingning Liu, Xiaoshui Huang, Yuenan Hou, Zhihui Wang, Zhenfei Yin, Yongshun Gong, Peng Gao, and Wanli Ouyang. Uni3d-llm: Unifying point cloud perception, generation and editing with large language models. *arXiv preprint arXiv:2402.03327*, 2024. 2
- [52] Quande Liu, Youpeng Wen, Jianhua Han, Chunjing Xu, Hang Xu, and Xiaodan Liang. Open-world semantic segmentation via contrasting and clustering vision-language embedding. In *European Conference on Computer Vision*, pages 275–292. Springer, 2022. 3
- [53] Shikun Liu, Edward Johns, and Andrew J Davison. End-to-end multi-task learning with attention. In *Proceedings of the IEEE/CVF conference on computer vision and pattern recognition*, pages 1871–1880, 2019. 5
- [54] Shilong Liu, Zhaoyang Zeng, Tianhe Ren, Feng Li, Hao Zhang, Jie Yang, Chunyuan Li, Jianwei Yang, Hang Su, Jun Zhu, et al. Grounding dino: Marrying dino with grounded pre-training for open-set object detection. *arXiv preprint arXiv:2303.05499*, 2023. 2, 6, 7, 9, 11, 23, 24
- [55] Yichen Liu, Benran Hu, Chi-Keung Tang, and Yu-Wing Tai. Sanerf-hq: Segment anything for nerf in high quality. In *Proceedings of the IEEE/CVF Conference on Computer Vision and Pattern Recognition*, pages 3216–3226, 2024. 3
- [56] Zhiheng Liu, Hao Ouyang, Qiuyu Wang, Ka Leong Cheng, Jie Xiao, Kai Zhu, Nan Xue, Yu Liu, Yujun Shen, and Yang Cao. Infusion: Inpainting 3d gaussians via learning depth completion from diffusion prior. *arXiv preprint arXiv:2404.11613*, 2024. 3

- [57] Ricardo Martin-Brualla, Noha Radwan, Mehdi SM Sajjadi, Jonathan T Barron, Alexey Dosovitskiy, and Daniel Duckworth. Nerf in the wild: Neural radiance fields for unconstrained photo collections. In *Proceedings of the IEEE/CVF conference on computer vision and pattern recognition*, pages 7210–7219, 2021. 1, 2
- [58] B Mildenhall, PP Srinivasan, M Tancik, JT Barron, R Ramamoorthi, and R Ng. Nerf: Representing scenes as neural radiance fields for view synthesis. In *European conference on computer vision*, 2020. 1, 2
- [59] Ashkan Mirzaei, Yash Kant, Jonathan Kelly, and Igor Gilitschenski. Laterf: Label and text driven object radiance fields. In *European Conference on Computer Vision*, pages 20–36. Springer, 2022. 3
- [60] Ashkan Mirzaei, Tristan Aumentado-Armstrong, Konstantinos G Derpanis, Jonathan Kelly, Marcus A Brubaker, Igor Gilitschenski, and Alex Levinshstein. Spin-nerf: Multiview segmentation and perceptual inpainting with neural radiance fields. In *Proceedings of the IEEE/CVF Conference on Computer Vision and Pattern Recognition*, pages 20669–20679, 2023. 1, 3
- [61] Heejoon Moon, Chunghwan Lee, and Je Hyeong Hong. Efficient privacy-preserving visual localization using 3d ray clouds. In *Proceedings of the IEEE/CVF Conference on Computer Vision and Pattern Recognition (CVPR)*, pages 9773–9783, 2024. 3
- [62] Arsalan Mousavian, Hamed Pirsiavash, and Jana Košecká. Joint semantic segmentation and depth estimation with deep convolutional networks. In *2016 Fourth International Conference on 3D Vision (3DV)*, pages 611–619. IEEE, 2016. 5
- [63] Thomas Müller, Alex Evans, Christoph Schied, and Alexander Keller. Instant neural graphics primitives with a multiresolution hash encoding. *ACM transactions on graphics (TOG)*, 41(4):1–15, 2022. 1, 2
- [64] James Munkres. Algorithms for the assignment and transportation problems. *Journal of the society for industrial and applied mathematics*, 5(1):32–38, 1957. 4
- [65] Milad Nasr, Saeed Mahloujifar, Xinyu Tang, Prateek Mittal, and Amir Houmansadr. Effectively using public data in privacy preserving machine learning. In *International Conference on Machine Learning*, pages 25718–25732. PMLR, 2023. 3
- [66] Maxime Oquab, Timothée Darcet, Théo Moutakanni, Huy Vo, Marc Szafraniec, Vasil Khalidov, Pierre Fernandez, Daniel Haziza, Francisco Massa, Alaaeldin El-Nouby, et al. Dinov2: Learning robust visual features without supervision. *Transactions on Machine Learning Research Journal*, pages 1–31, 2024. 3
- [67] Songyou Peng, Kyle Genova, Chiyu Jiang, Andrea Tagliasacchi, Marc Pollefeys, Thomas Funkhouser, et al. Openscene: 3d scene understanding with open vocabularies. In *Proceedings of the IEEE/CVF conference on computer vision and pattern recognition*, pages 815–824, 2023. 1, 2
- [68] Francesco Pittaluga, Sanjeev J Koppal, Sing Bing Kang, and Sudepta N Sinha. Revealing scenes by inverting structure from motion reconstructions. In *Proceedings of the IEEE/CVF Conference on Computer Vision and Pattern Recognition*, pages 145–154, 2019. 3
- [69] Minghan Qin, Wanhua Li, Jiawei Zhou, Haoqian Wang, and Hanspeter Pfister. Langsplat: 3d language gaussian splatting. In *Proceedings of the IEEE/CVF Conference on Computer Vision and Pattern Recognition*, pages 20051–20060, 2024. 3
- [70] Alec Radford, Jong Wook Kim, Chris Hallacy, Aditya Ramesh, Gabriel Goh, Sandhini Agarwal, Girish Sastry, Amanda Askell, Pamela Mishkin, Jack Clark, et al. Learning transferable visual models from natural language supervision. In *International conference on machine learning*, pages 8748–8763. PmlR, 2021. 1, 3, 6
- [71] Hugo Raguét. A note on the forward-Douglas–Rachford splitting for monotone inclusion and convex optimization. *Optimization Letters*, pages 1–24, 2018. 6, 11
- [72] Hugo Raguét and Loïc Landrieu. Preconditioning of a generalized forward-backward splitting and application to optimization on graphs. *SIAM Journal on Imaging Sciences*, 8(4):2706–2739, 2015. 6, 11
- [73] Nikhil Raina, Guruprasad Somasundaram, Kang Zheng, Sagar Miglani, Steve Saarinen, Jeff Meissner, Mark Schwesinger, Luis Pesqueira, Ishita Prasad, Edward Miller, Prince Gupta, Mingfei Yan, Richard Newcombe, Carl Ren, and Omkar M Parkhi. Egoblur: Responsible innovation in aria, 2023. 3
- [74] Nikhila Ravi, Valentin Gabeur, Yuan-Ting Hu, Ronghang Hu, Chaitanya Ryali, Tengyu Ma, Haitham Khedr, Roman Rädle, Chloe Rolland, Laura Gustafson, Eric Mintun, Junting Pan, Kalyan Vasudev Alwala, Nicolas Carion, Chao-Yuan Wu, Ross Girshick, Piotr Dollár, and Christoph Feichtenhofer. Sam 2: Segment anything in images and videos. *arXiv preprint arXiv:2408.00714*, 2024. 3, 4
- [75] RealityCapture2023. RealityCapture, 2023. 1
- [76] Christian Reiser, Songyou Peng, Yiyi Liao, and Andreas Geiger. Kilonerf: Speeding up neural radiance fields with thousands of tiny mlps. In *Proceedings of the IEEE/CVF international conference on computer vision*, pages 14335–14345, 2021. 1, 2
- [77] Tianhe Ren, Shilong Liu, Ailing Zeng, Jing Lin, Kunchang Li, He Cao, Jiayu Chen, Xinyu Huang, Yukang Chen, Feng Yan, Zhaoyang Zeng, Hao Zhang, Feng Li, Jie Yang, Hongyang Li, Qing Jiang, and Lei Zhang. Grounded sam: Assembling open-world models for diverse visual tasks, 2024. 2, 6, 7, 9, 11, 23, 24
- [78] Robin Rombach, Andreas Blattmann, Dominik Lorenz, Patrick Esser, and Björn Ommer. High-resolution image synthesis with latent diffusion models. In *Proceedings of the IEEE/CVF conference on computer vision and pattern recognition*, pages 10684–10695, 2022. 3
- [79] Ira S Rubinstein and Nathaniel Good. Privacy by design: A counterfactual analysis of google and facebook privacy incidents. *Berkeley Tech. LJ*, 28:1333, 2013. 3
- [80] Chitwan Saharia, William Chan, Saurabh Saxena, Lala Li, Jay Whang, Emily L Denton, Kamyar Ghasemipour, Raphael Gontijo Lopes, Burcu Karagol Ayan, Tim Salimans, et al. Photorealistic text-to-image diffusion models

- with deep language understanding. *Advances in neural information processing systems*, 35:36479–36494, 2022. 3
- [81] Johannes L Schonberger and Jan-Michael Frahm. Structure-from-motion revisited. In *Proceedings of the IEEE conference on computer vision and pattern recognition*, pages 4104–4113, 2016. 2, 6
- [82] Johannes Lutz Schönberger, Enliang Zheng, Marc Pollefeys, and Jan-Michael Frahm. Pixelwise view selection for unstructured multi-view stereo. In *European Conference on Computer Vision (ECCV)*, 2016. 2
- [83] Christoph Schuhmann, Romain Beaumont, Richard Vencu, Cade Gordon, Ross Wightman, Mehdi Cherti, Theo Coombes, Aarush Katta, Clayton Mullis, Mitchell Wortsman, et al. Laion-5b: An open large-scale dataset for training next generation image-text models. *Advances in neural information processing systems*, 35:25278–25294, 2022. 1
- [84] Jin-Chuan Shi, Miao Wang, Hao-Bin Duan, and Shao-Hua Guan. Language embedded 3d gaussians for open-vocabulary scene understanding. In *Proceedings of the IEEE/CVF Conference on Computer Vision and Pattern Recognition*, pages 5333–5343, 2024. 1, 3
- [85] Yawar Siddiqui, Lorenzo Porzi, Samuel Rota Buló, Norman Müller, Matthias Nießner, Angela Dai, and Peter Kotschieder. Panoptic lifting for 3d scene understanding with neural fields. In *Proceedings of the IEEE/CVF Conference on Computer Vision and Pattern Recognition*, pages 9043–9052, 2023. 3
- [86] Pablo Speciale, Johannes L Schonberger, Sing Bing Kang, Sudipta N Sinha, and Marc Pollefeys. Privacy preserving image-based localization. In *Proceedings of the IEEE/CVF Conference on Computer Vision and Pattern Recognition*, pages 5493–5503, 2019. 3
- [87] Ayca Takmaz, Alexandros Delitzas, Robert W Sumner, Francis Engelmann, Johanna Wald, and Federico Tombari. Search3d: Hierarchical open-vocabulary 3d segmentation. *IEEE Robotics and Automation Letters*, 2025. 1
- [88] Matthew Tancik, Ethan Weber, Evonne Ng, Ruilong Li, Brent Yi, Justin Kerr, Terrance Wang, Alexander Kristoffersen, Jake Austin, Kamyar Salahi, Abhik Ahuja, David McAllister, and Angjoo Kanazawa. Nerfstudio: A modular framework for neural radiance field development. In *ACM SIGGRAPH 2023 Conference Proceedings*, 2023. 1
- [89] Vadim Tschernezki, Iro Laina, Diane Larlus, and Andrea Vedaldi. Neural feature fusion fields: 3d distillation of self-supervised 2d image representations. In *2022 International Conference on 3D Vision (3DV)*, pages 443–453. IEEE, 2022. 3
- [90] Paul Voigt and Axel Von dem Bussche. The eu general data protection regulation (gdpr). *A practical guide, 1st ed., Cham: Springer International Publishing*, 10(3152676): 10–5555, 2017. 3, 9
- [91] Suhani Vora*, Noha Radwan*, Klaus Greff, Henning Meyer, Kyle Genova, Mehdi S. M. Sajjadi, Etienne Pot, Andrea Tagliasacchi, and Daniel Duckworth. Nesf: Neural semantic fields for generalizable semantic segmentation of 3d scenes. *Transactions on Machine Learning Research*, 2022. 3
- [92] Can Wang, Menglei Chai, Mingming He, Dongdong Chen, and Jing Liao. Clip-nerf: Text-and-image driven manipulation of neural radiance fields. In *Proceedings of the IEEE/CVF conference on computer vision and pattern recognition*, pages 3835–3844, 2022. 3
- [93] Yunsong Wang, Tianxin Huang, Hanlin Chen, and Gim Hee Lee. Freesplat: Generalizable 3d gaussian splatting towards free view synthesis of indoor scenes. *Advances in Neural Information Processing Systems*, 37:107326–107349, 2024. 1, 2
- [94] Silvan Weder, Guillermo Garcia-Hernando, Aron Monszpart, Marc Pollefeys, Gabriel J Brostow, Michael Firman, and Sara Vicente. Removing objects from neural radiance fields. In *Proceedings of the IEEE/CVF Conference on Computer Vision and Pattern Recognition*, pages 16528–16538, 2023. 3
- [95] Yanmin Wu, Jiarui Meng, LI Haijie, Chenming Wu, Yahao Shi, Xinhua Cheng, Chen Zhao, Haocheng Feng, Errui Ding, Jingdong Wang, et al. Opengaussian: Towards point-level 3d gaussian-based open vocabulary understanding. In *The Thirty-Eighth Annual Conference on Neural Information Processing Systems (NeurIPS 2024)*, 2024. 1
- [96] Yanmin Wu, Jiarui Meng, Haijie Li, Chenming Wu, Yahao Shi, Xinhua Cheng, Chen Zhao, Haocheng Feng, Errui Ding, Jingdong Wang, et al. Opengaussian: Towards point-level 3d gaussian-based open vocabulary understanding. 2024. 3
- [97] Mingqiao Ye, Martin Danelljan, Fisher Yu, and Lei Ke. Gaussian grouping: Segment and edit anything in 3d scenes. In *ECCV*, 2024. 1, 3, 6, 7, 8, 9, 11, 12, 13, 15, 16, 23, 24, 27, 28
- [98] Vickie Ye, Ruilong Li, Justin Kerr, Matias Turkulainen, Brent Yi, Zhuoyang Pan, Otto Seiskari, Jianbo Ye, Jeffrey Hu, Matthew Tancik, and Angjoo Kanazawa. gsplat: An open-source library for Gaussian splatting. *arXiv preprint arXiv:2409.06765*, 2024. 1
- [99] Yingda Yin, Yuzheng Liu, Yang Xiao, Daniel Cohen-Or, Jingwei Huang, and Baoquan Chen. Sai3d: Segment any instance in 3d scenes. In *Proceedings of the IEEE/CVF Conference on Computer Vision and Pattern Recognition*, pages 3292–3302, 2024. 2
- [100] Zehao Yu, Anpei Chen, Bozidar Antic, Songyou Peng, Apratim Bhattacharyya, Michael Niemeyer, Siyu Tang, Torsten Sattler, and Andreas Geiger. Sdfstudio: A unified framework for surface reconstruction, 2022. 1
- [101] Zehao Yu, Torsten Sattler, and Andreas Geiger. Gaussian opacity fields: Efficient adaptive surface reconstruction in unbounded scenes. *ACM Transactions on Graphics (TOG)*, 43(6):1–13, 2024. 1, 2
- [102] Tong He Hengshuang Zhao Yunhan Yang, Xiaoyang Wu and Xihui Liu. Sam3d: Segment anything in 3d scenes. In *ICCVW*, 2023. 2
- [103] Ramin Zabih and Vladimir Kolmogorov. Spatially coherent clustering using graph cuts. In *Proceedings of the 2004 IEEE Computer Society Conference on Computer Vision and Pattern Recognition, 2004. CVPR 2004.*, pages II–II. IEEE, 2004. 5

- [104] Dongbin Zhang, Chuming Wang, Weitao Wang, Peihao Li, Minghan Qin, and Haoqian Wang. Gaussian in the wild: 3d gaussian splatting for unconstrained image collections. In *European Conference on Computer Vision*, pages 341–359. Springer, 2024. [1](#), [2](#)
- [105] Shuaifeng Zhi, Tristan Laidlow, Stefan Leutenegger, and Andrew J Davison. In-place scene labelling and understanding with implicit scene representation. In *Proceedings of the IEEE/CVF International Conference on Computer Vision*, pages 15838–15847, 2021. [3](#)
- [106] Shijie Zhou, Haoran Chang, Sicheng Jiang, Zhiwen Fan, Zehao Zhu, Dejia Xu, Pradyumna Chari, Suyu You, Zhangyang Wang, and Achuta Kadambi. Feature 3dgs: Supercharging 3d gaussian splatting to enable distilled feature fields. In *Proceedings of the IEEE/CVF Conference on Computer Vision and Pattern Recognition*, pages 21676–21685, 2024. [1](#), [3](#), [5](#), [6](#), [7](#), [8](#), [9](#), [11](#), [12](#), [13](#), [14](#), [15](#), [16](#), [17](#), [19](#), [20](#), [24](#), [27](#), [28](#)
- [107] Xueyan Zou, Jianwei Yang, Hao Zhang, Feng Li, Linjie Li, Jianfeng Wang, Lijuan Wang, Jianfeng Gao, and Yong Jae Lee. Segment everything everywhere all at once. *Advances in neural information processing systems*, 36: 19769–19782, 2023. [3](#)
- [108] Xingxing Zuo, Pouya Samangouei, Yunwen Zhou, Yan Di, and Mingyang Li. Fmgs: Foundation model embedded 3d gaussian splatting for holistic 3d scene understanding. *International Journal of Computer Vision*, pages 1–17, 2024. [3](#)